Response to RC2:

Authors: Xirui Ma, Yun Zhang, Panyan Ge, Yan Yin, Hepeng Zheng, Tingting Kang, Lingbing Bu, Wenjie Su, Donglin Yang, Qiangyue Xiang and Yinze Ran

We greatly appreciate your valuable time for reviewing our research paper and providing suggestions. ***(The blue text is in response to your comments, and the green text is for specific modifications in the paper. We also highlight revisions in the manuscript.)***

General Review:

This manuscript uses a case study event at Qingbang Island in the East China Sea to investigate the potential impacts of transported dust aerosol on the formation and evolution of sea fog. The case study was explored using station observations of meteorological variables, radiation, turbulence, and particulate matter concentrations; Himawari-9 fog and aerosol retrievals; and ERA5 reanalysis to establish large-scale conditions. The study period was divided into 7 stages, beginning just prior to the arrival of transported dust aerosol and ending with the dissipation of fog and mist. These stages were used to organize the observational analysis.

The topic is scientifically valuable, given the large uncertainties in aerosol – sea fog interactions and complex mechanisms at play. Observational case studies can provide valuable insight into these processes and the experimental design of this study has promise. However, I am concerned that the analysis presented here is insufficient to support the authors' conclusions.

My concerns can be grouped into two categories: those that may simply be a matter of presentation (e.g. vague methodology, inconsistent use of measurement precision, and inappropriate descriptions of measured trends, which may represent flaws in the underlying analysis or may simply be a question of writing style) and those where the authors claims are unsupported by or inconsistent with the presented evidence.

Answer:

We sincerely appreciate the reviewer's valuable comments and suggestions. We have carefully revised the manuscript and figures in accordance with the specific recommendations provided.

Specific Comments:

- **Throughout, the evolution of the case study event is interpreted from imagery on maps which show a very large geographic area – so large that we cannot actually see what is happening around the measurement site. It is thus difficult to assess the credibility of the claims being made.**

Answer: We highly appreciate the reviewer's constructive suggestion, which indeed helps to improve the readability and focus of the figures. We have addressed this point through the following revisions and clarifications:

(1). We have redrawn Figure 1 accordingly, which significantly improves the geographical context of our study area. The revised results are as follows:

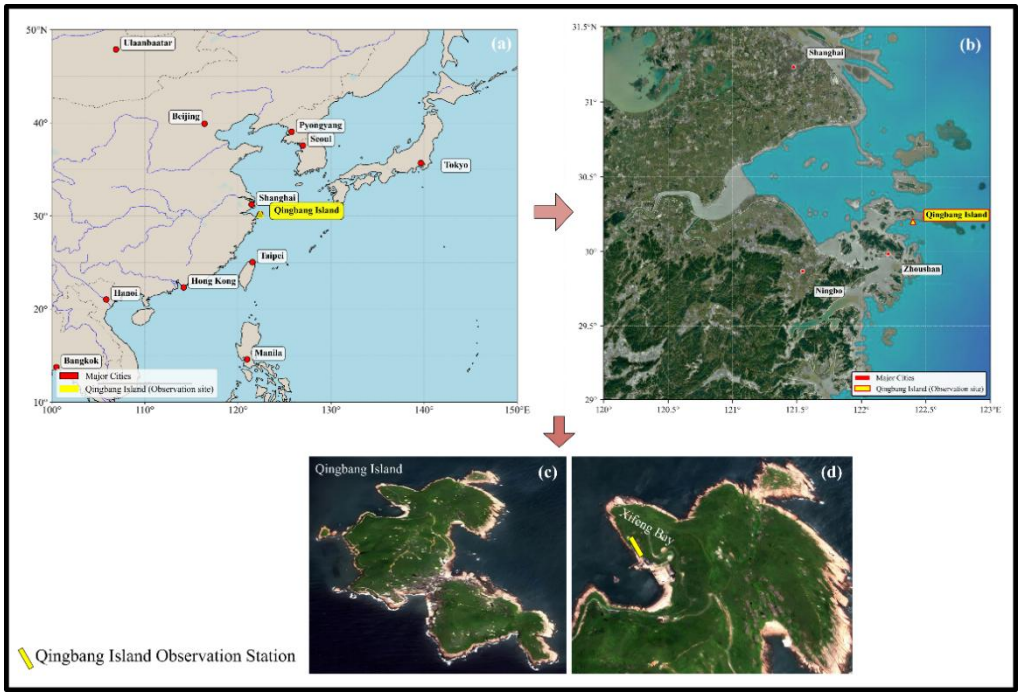

(2). We have reduced the drawing area for Figures 2 and 4 in the original manuscript. However, for Figure 12, we have retained the original drawing range of the figure. The formation of this advection sea fog and the long-range transport of dust aerosols are deeply driven by synoptic-scale circulation patterns (e.g., the Mongolian cyclone and westerly jet). Keeping a broader regional domain in Figure 12 is physically essential to fully illustrate the macro-scale atmospheric forcing, the origins of the air masses, and the complete transport pathways of the dust from inland to the ocean. We kindly ask the reviewer to appreciate that, due to the synoptic-scale nature of the analysis, the larger plotting domain of Figure 12 is retained. The revised results are as follows:

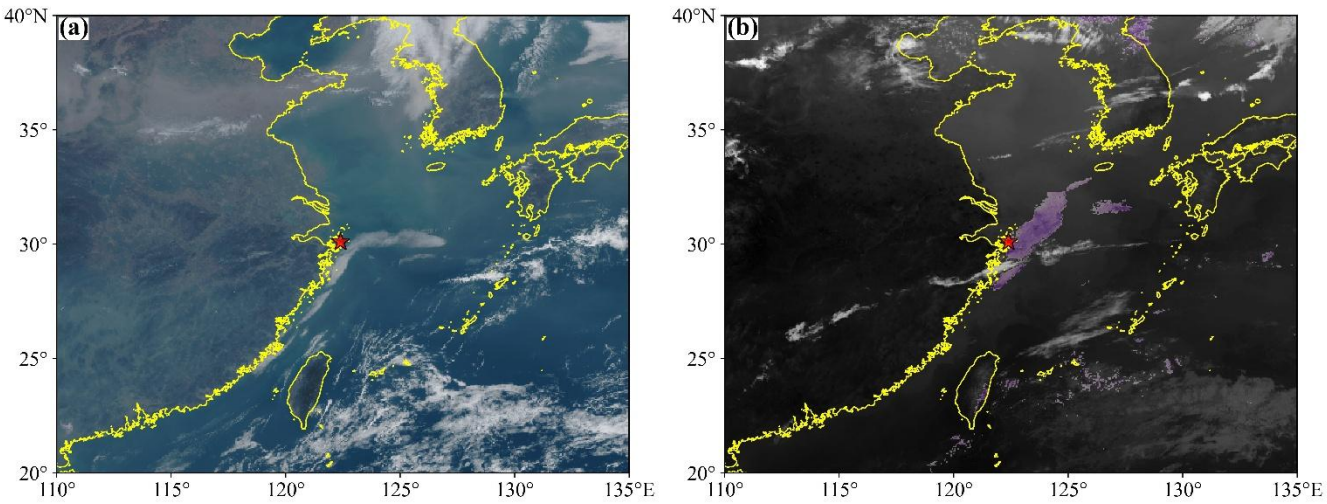

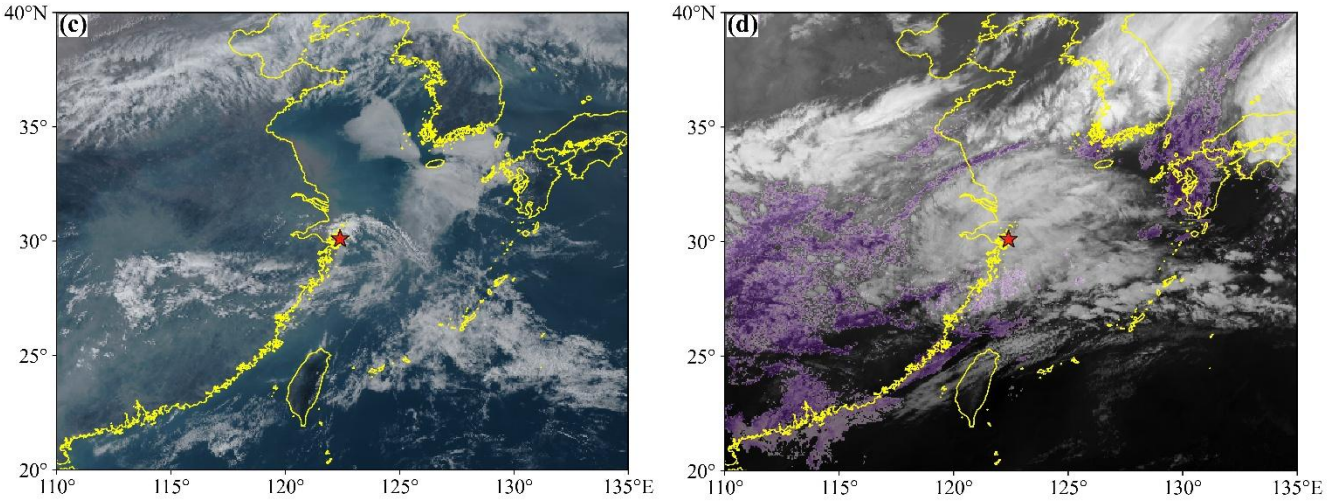

Figure 2: Sea fog monitoring images from the H-9 satellite at four different times. Sea fog is identified using different channels during the day and at night. a and c are the AHI RGB true-colour images composited from the visible channels at 09:00 LST on March 25 and 15:00 LST on March 26, respectively (local standard time (LST) = Universal Time Coordinated (UTC) + 8 h). b and d are the nighttime sea fog identification images obtained by the brightness temperature difference method using the infrared channels, since the visible channels are unavailable at night, at 18:00 LST on March 25 and 00:00 LST on March 28, respectively. Purple indicates fog identified at nighttime. The red star indicates the observation site.

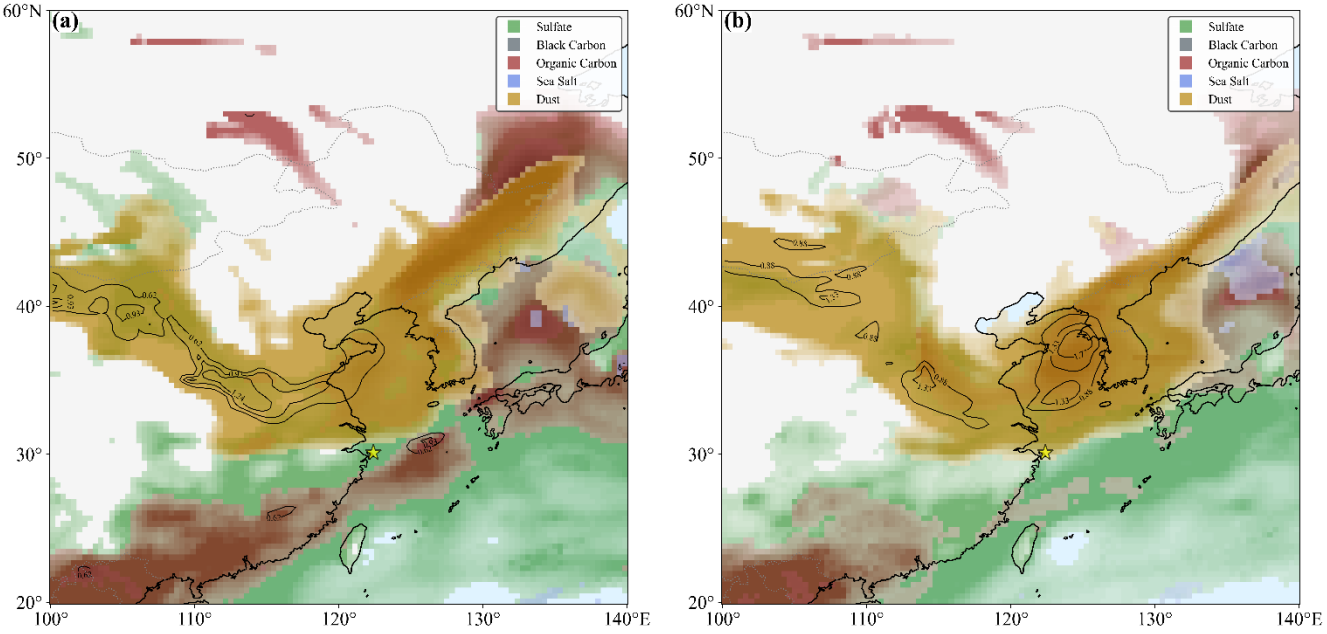

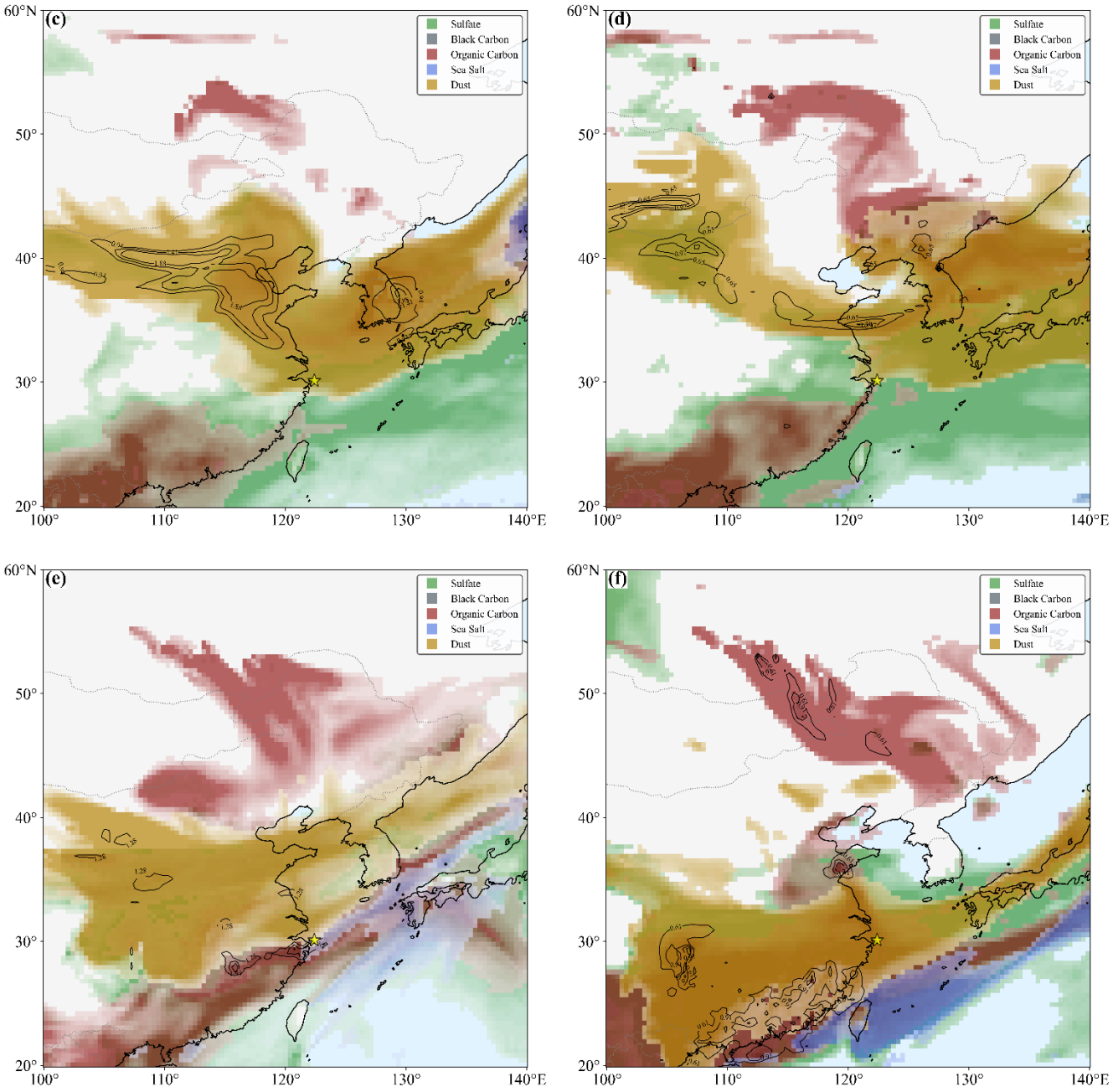

Figure 4: Panels show the distribution of aerosol types at (a) 08:00 LST on March 24 (Stage 1: pre-dust phase), (b) 15:00 LST on March 24 (Stage 2: dust phase), (c) 00:00 LST on March 25 (Stage 3: pre-formation phase of advection sea fog), (d) 15:00 LST on March 25 (Stage 3: pre-formation phase of advection sea fog), (e) 18:00 LST on March 27 (Stage 7: dissipation phase of mist), and (f) 18:00 LST on March 28 (Stage 7: dissipation phase of mist). In the figure, green, gray, red, blue, and yellow represent sulfate, black carbon, organic carbon, sea salt, and dust aerosols, respectively. The yellow star indicates the observation site.

- **A number of methodological descriptions require more detail:**

- **L122-124: "To eliminate high-frequency random noise… all surface meteorological elements were subjected to strict quality control." Please elaborate on the quality control applied.**

Answer: we sincerely thank the reviewer for this excellent suggestion. According to your advice, the content on line 122-124 of the original manuscript has been revised as follows:

To address the scarcity of high-spatiotemporal-resolution meteorological data in this marine region, we deployed an automatic weather station (AWS) to collect raw observational data at a 10-second temporal resolution. The main observation parameters include air temperature (T), relative humidity (RH), pressure (Pa), wind speed (WS), wind direction (WD), particulate matter mass concentration (PM_1、$PM_{2.5}$、PM_{10}), and visibility (Vis). To eliminate high-frequency random noise and ensure data stability, all surface meteorological elements were subjected to strict quality control. The specific procedures included: (1) physical limit checks to remove physically impossible values (e.g., relative humidity > 100% or < 0%, or negative wind speeds). (2) spike detection to eliminate isolated high-frequency noise and sudden unrealistic jumps. (3) constant value checks to remove invalid data caused by temporary sensor malfunctions. Finally, the processed data were averaged into time series with 1-min intervals for subsequent analysis. The PM mass concentration measurement equipment used in this study performs sampling by heating the drawn-in air and reducing its relative humidity to below 40%. Specifically, ambient air is drawn in by a sampling pump at a constant flow rate, and before entering the optical measurement chamber, its relative humidity is reduced to below 40% through a heating tube, ensuring the particles are in a dry state during measurement. The measured PM_1, $PM_{2.5}$, and PM_{10} correspond to the dry aerosol mass, effectively eliminating the direct interference from liquid fog droplets and the moisture of hydrated particles.

- **L128-129: "Vertical profiles … were obtained through retrieval algorithms." Please elaborate on the retrieval algorithms used and whether the results are a published or custom product.**

Answer: We sincerely appreciate the reviewer's professional and insightful question regarding the microwave radiometer (MWR) data. The content in line 128-129 of the text has also been elaborately supplemented. The content on line 28-129 of the original manuscript has been revised as follows:

Radiation parameters were measured by a four-component radiometer (CNR4). This instrument can simultaneously measure downward shortwave radiation (DSR), upward shortwave radiation (USR), downward longwave radiation (DLR), and upward longwave radiation (ULR). Net radiation (Rn) was calculated based on the surface radiation balance equation: Rn = (DSR - USR) + (DLR - ULR). To match the analysis scale of boundary layer fluxes, all radiation component data were processed into 30-min averages. In addition, a ground-based microwave radiometer (RPG-HATPRO) was used. Vertical profiles of air temperature in the boundary layer with high temporal resolution were obtained through retrieval algorithms. Vertical profiles of air temperature in the boundary layer were retrieved using a Neural Network (NN) algorithm based on the observed radiation brightness temperatures of oxygen molecules. To ensure optimal regional accuracy and representativeness, the NN algorithm was systematically trained using a localized dataset comprising 10 years of historical balloon-borne radiosonde observations.

- **L282: "… the bilinear interpolation method was used." What is being interpolated? Is this an interpolation in space to obtain values at the study location? In time to obtain a continuous dataset?**

Answer: We thank the reviewer for this question. The bilinear interpolation method used here is for the AOD of different types of aerosols. This is a spatial interpolation, not a temporal interpolation.

To further study the impact of aerosols on the formation and dissipation mechanism of this sea fog, based on the aerosol component AOD product of the H-9 satellite, the bilinear interpolation method was used to spatially interpolate the AOD onto the location of the observation site. The temporal variation characteristics of AOD for sulfate, black carbon, organic carbon, sea salt, and dust aerosols at Qingbang Island in the East China Sea were thereby calculated (Fig. 5(a)). Based on this, the average contribution rates of different types of aerosols during the entire study period were calculated (Fig. 5(b)). In this study, satellite derived aerosol composition data are utilized as quantitative observations during Stages 1–3 and 7, whereas they are limited to qualitative reference during the fog period (Stages 4–6).

- **Measurement uncertainties and statistics are inadequately considered, and temporal behaviour is inappropriately described. E.g.,**

- **Descriptions of Stages 1-7: no measurement uncertainties are quoted.**

Answer: We thank the reviewer for this question. We note that, although the measurement ranges and specified accuracies (i.e., the measurement uncertainties) of the instruments are already listed in Table 1, we did not explicitly relate these uncertainties to the specific observed values when reporting them in Stages 1–7. Accordingly, we have added a general statement on line 206 of the original manuscript has been revised as follows:

> Based on the fog identification criteria of WMO (WMO/GAW, 2003) and the UK Met Office (Met Office, 1994) (Vis < 1 km and RH ≥ 95% is identified as fog, 1 km ≤ Vis ＜ 5 km and RH ≥ 95% is identified as mist). This event was divided into 7 detailed stages (Table 2). Table 2 shows the sequence numbers, stage name, time, visibility, and relative humidity of the 7 stages. The measurement uncertainties of the near-surface observations for stages 1–7 are based on the instrumental accuracies listed in Table 1. The magnitudes of the variations discussed below all exceed their respective measurement uncertainties.

- **L222 (description of Stage 2): "The visibility dropped sharply by 28.4% to 1.79km." By eye, the reduction in visibility in Stage 2 is smaller than the noise in Stage 1. What reference value is 28.4% calculated relative to? I assume that 1.79km is the minimum value reached during Stage 1 since it is neither the first, last, nor average (per Table 2); if comparing a minimum to a mean, be explicit about this. I also disagree with the characterization that visibility "dropped sharply;" rather, it trends downwards through Stage 1 until it reaches a minimum in the middle of Stage 2.**

Answer: We thank the reviewer for the careful reading. On checking, we acknowledge that this sentence in the original manuscript was not stated rigorously and caused confusion; we correct it as follows:

(1) Reference value for the 28.4%: the original text did not state the reference value, which is now added. The value is calculated relative to the visibility of 2.5 km at the beginning of Stage 2 (Table 2), i.e., (2.5 − 1.79)/2.5 × 100% ≈ 28.4%.

(2) Meaning of 1.79 km: this is the visibility at the moment when the dust arrived and the PM concentration peaked (17:08), i.e., an instantaneous local minimum in the middle of Stage 2, and not a minimum reached during Stage 1. The ambiguity arose because the original text did not indicate the time to which this value corresponds.

(3) On "dropped sharply": we agree that this wording is inappropriate. The visibility had been decreasing since Stage 1 and reached a local minimum in the middle of Stage 2 (at the PM peak), rather than dropping sharply. We have revised it to an objective statement, and have also changed "strict inverse trend" to "inverse trend." The revised text is shown above.

The content on line 222 of the original manuscript has been revised as follows:

Stage 2 was affected by strong external disturbance. The PM mass concentrations showed explosive increases during this period. The peak values of PM_1, $PM_{2.5}$, and PM_{10} at 17:08 on March 24 were 267, 460, and 469 μg/m³, respectively (an increase of 11-14 times). This trend is consistent with the explosive input characteristics of dust aerosols (Rodríguez et al., 2024). During this stage, the average visibility was 2.4 km and the relative humidity remained at a low level of 40-65% (Table 2). At the PM peak, the visibility decreased to a local minimum of 1.8 km, a reduction of 28% relative to the visibility of 2.5 km at the beginning of Stage 2 (Table 2), showing a strict inverse trend with PM mass concentration changes. The PM mass concentration peak (17:08) was synchronous with the wind speed peak (6.3 m/s). In addition, the event occurred during a concurrent cold-air intrusion in late March, within the dust season. These strongly coupled surface features are similar to those of long-range dust transport. Therefore, in conjunction with the satellite data and circulation analysis evidence presented in subsequent sections (Sections 3.2 and 3.5), this stage is identified as the dust passage period. It should be noted that, based on the PM mass concentrations available in this study, we cannot physically or quantitatively separate the respective contributions of the $PM_{2.5}$ and the dust. The dust impact discussed hereafter therefore refers to the overall synergistic effect of this long range transported, dust-dominated dust–pollution air mass treated as a whole. The cold-air intrusion combined with the dust radiative effects intensified the near-surface temperature drop (a decrease of 5.0°C within

5 hours, with a cooling rate of about 1.0°C/h). In addition, the pressure showed an increase during 16:27-20:00. This may be related to the thermodynamic pressurization effect of aerosol increase on the local boundary layer (Luo et al., 2022).

- **Reported measurements have inconsistent precision. Eg in Sec 3.1, visibility measurements are quoted to the nearest 1, 0.1, and 0.01 km. Similarly, "wind speed increased from 6.4 to 9 m/s" should use the same number of significant figures on the two values.**

Answer: We thank the reviewer for this question. We agree that reported measurements should be quoted with consistent precision. On checking, we have made the following unifications:

(1) Visibility: we have standardized the visibility measurements in Section 3.1 to one decimal place (i.e., 0.1 km), commensurate with the specified accuracy of the visibility sensor (±5%, Table 1). Accordingly, the 1.79 km in the original text has been changed to 1.8 km, and the corresponding percentage reduction derived from it has been adjusted to about 28%. We note that the thresholds in the fog/mist criteria (Vis < 1 km, 1 km ⩽ Vis < 5 km) are the nominal definitional values of the WMO and UK Met Office criteria, not measured readings, and are therefore kept as originally defined.

(2) Consistency of significant figures within a statement: we have unified paired values such as wind speeds to the same number of significant figures; for example, "wind speed increased from 6.4 to 9 m/s" has been changed to "from 6.4 to 9.0 m/s."

The content on line 215-254 of the original manuscript has been revised as follows:

Stage 2 was affected by strong external disturbance. The PM mass concentrations showed explosive increases during this period. The peak values of PM_1, $PM_{2.5}$, and PM_{10} at 17:08 on March 24 were 267, 460, and 469 μg/m³, respectively (an increase of 11-14 times). This trend is consistent with the explosive input characteristics of dust aerosols (Rodríguez et al., 2024). During this stage, the average visibility was 2.4 km and the relative humidity remained at a low level of 40-65% (Table 2). At the PM peak, the visibility decreased to a local minimum of 1.8 km, a reduction of 28% relative to the visibility of 2.5 km at the beginning of Stage 2 (Table 2), showing a strict inverse trend with PM mass concentration changes. The PM mass concentration peak (17:08) was synchronous with the wind speed peak (6.3 m/s). In addition, the event occurred during a concurrent cold-air intrusion in late March, within the dust season. These strongly coupled surface features are similar to those of long-range dust transport. Therefore, in conjunction with the satellite data and circulation analysis evidence presented in subsequent sections (Sections 3.2 and 3.5), this stage is identified as the dust passage period. It should be noted that, based on the PM mass concentrations available in this study, we cannot physically or quantitatively separate the respective contributions of the $PM_{2.5}$ and the dust. The dust impact discussed hereafter therefore refers to the overall synergistic effect of this long range transported, dust-dominated dust–pollution air mass treated as a whole. The cold-air intrusion combined with the dust radiative effects intensified the near-surface temperature drop (a decrease of 5.0°C within 5 hours, with a cooling rate of about 1.0°C/h). In addition, the pressure showed an increase during 16:27-20:00. This may be related to the thermodynamic pressurization effect of aerosol increase on the local boundary layer (Luo et al., 2022).

The system then entered the coupling period of the core mechanism of sea fog outbreak, including Stage 3 and Stage 4. At the beginning of Stage 3, the residual dust aerosols showed a gentle oscillating decrease. The settling rate of PM_{10} was about 2 μg/m³/h, which is consistent with the gravitational settling model. The PM mass concentrations increased during 12:32-16:47 on March 25. This may be related to the hygroscopic growth of aerosol particles. During 04:30-09:00 on March 25, the near-surface wind at the site remained predominantly southerly. After 09:00 on March 25, the wind speed continued to increase to 6.0 $m \cdot s^{-1}$ with continuous warm and moist advection. This provided sufficient water vapor transport for sea fog outbreak. It was favourable for the hygroscopic growth of settled dust and other aerosols to prepare for sea fog outbreak. At the end of Stage 3 (16:20-16:47), the thermodynamic conditions changed obviously. The temperature cooling rate was about 2.9°C/h, and the RH jumped to 100%. At the same time, the pressure turned to a weak increase after reaching the bottom since 15:30 on March 25. This indicates that the overall environmental field (thermal and dynamic background) changed. The combined effect of thermal and dynamic condition changes finally led to a sharp decrease in visibility to 1.0 km at 16:47 on March 25. During Stage 4, the visibility decreased sharply. The minimum visibility was 0.3 km. The aerosol concentrations showed a significant increase with multi-peak fluctuation characteristics.

The system attenuation began in Stage 5, which was still under the conditions of RH at 100% and stable southerly wind. The PM mass concentrations showed a three-peak decreasing trend, and the decreasing rate showed PM_{10} > $PM_{2.5}$ > PM_1. This was closely related to the efficient removal of coarse aerosol particles by the gravitational collision and wet deposition of fog droplets. The atmospheric visibility was basically maintained at about 1.0 km, consistent with the alternating evolution trend of advection sea fog and mist. In Stage 6, the stable southerly wind drove the RH to remain at 95%-100%. A dynamic balance was formed between warm and moist advection and highly hygroscopic aerosols. The mist state was maintained for 33 hours (visibility 2.0-4.0 km). A dense fog disturbance event of nearly 1 hour occurred during this stage. During 08:08-09:05 on March 27, PM_{10} suddenly increased to 131 μg/m³. The visibility dropped sharply to 0.4 km. The wind speed increased to 5.8 m/s. After 09:25 on March 27, the northwest wind intruded. The intrusion of dry and cold air caused significant cooling. The RH dropped to the critical value of 95%. This caused the mist system to collapse (visibility increased to 4.0 km).

In the final Stage 7, driven by the continuously strengthening of the northwest wind, the dry and cold air mass completely replaced the warm and moist marine air mass. This caused the RH to drop from 95% to 77%, breaking the phase transition critical value of aerosols. In the early period from 17:50 to 19:00 on March 27, the wind speed increased from 6.4 to 9.0 m/s. This enhanced the turbulent vertical mixing and mechanically destroyed the residual fog droplets. The average mass concentrations of PM_1, $PM_{2.5}$, and PM_{10} in this stage decreased by 30%, 28%, and 25%, respectively, compared to those in Stage 6. The visibility continued to increase to 30.0 km, indicating the irreversible dissipation of the mist system.

- **Variability is over-described in ways that ascribe it artificial significance, e.g. L240: "The PM mass concentrations showed a three-peak decreasing trend" (unless these peaks have particular significance, perhaps better just to call it a "decreasing trend"?)**

Answer: We thank the reviewer for this comment. The content on line 240 of the original manuscript has been revised as follows:

The system attenuation began in Stage 5, which was still under the conditions of RH at 100% and stable southerly wind. The PM mass concentrations showed a decreasing trend, and the decreasing rate showed PM_{10} > $PM_{2.5}$ > PM_1.

. • **Throughout, "oscillating" is frequently used to described timeseries behaviour, eg L211 "… first increasing and then oscillating downward…" L227 "… a gentle oscillating decrease…" L349 "…a balanced oscillating trend" L482 "… the system entered a strong non-steady oscillation period…" This is a poor word choice since "oscillating" implies harmonic motion. In most cases, the term could simply be omitted, since trends are not necessarily linear or monotonic.**

Answer: We highly appreciate the reviewer's constructive suggestion. We agree that "oscillating" physically implies (quasi-)harmonic, periodic back-and-forth motion, whereas in most places in the manuscript it was used to describe non-monotonic fluctuations without a fixed period, which is imprecise. We have checked and revised each instance:

(1) At L211 (RH of Stage 1) and L227 (the settling of initial residual dust in Stage 3), the descriptions respectively depict the downward trend influenced by daytime radiation and the swirling of dry air, as well as the monotonic attenuation in accordance with the gravity settling model, all of which do not exhibit periodicity. We have removed "oscillating" and replaced it with "decreasing" and "a gentle decrease".

(2) At L349 (the proportion of various particle sizes in Stage 6 at the early stage), it describes a roughly balanced fluctuation without a monotonic trend. We have changed it to "remained in a relatively balanced state without a monotonic trend" to more accurately express its nonlinear and non-monotonic characteristics.

(3) Regarding L482: The Stage 6 described here represents the light fog persistence stage, which is a transitional phase where the system shifts from stability to dissipation. During this stage, factors such as warm moist advection, dry cold intrusion, and enhanced turbulence compete with each other, repeatedly disrupting the quasi-equilibrium of the system, and gradually reducing its stability until it eventually destabilizes and enters the dissipation stage 7. This process causes the observed data to exhibit a back-and-forth fluctuating characteristic; we agree that this fluctuation is not a strict periodic (harmonic) motion. Therefore, in accordance with the reviewers' suggestion, it has been rephrased as "non-steady period"

The content on line 211 of the original manuscript has been revised as follows:

The RH showed a trend of first increasing and then decreasing due to the enhancement of solar radiation and dry air entrainment.

The content on line 227 of the original manuscript has been revised as follows:

The system then entered the coupling period of the core mechanism of sea fog outbreak, including Stage 3 and Stage 4. At the beginning of Stage 3, the residual dust aerosols showed a gentle decrease.

The content on line 349 of the original manuscript has been revised as follows:

In the early period of Stage 6, the proportions of particles with sizes of 0-1, 1-2.5, and 2.5-10 μm basically remained in a relatively balanced state without a monotonic trend.

The content on line 482 of the original manuscript has been revised as follows:

Subsequently, the system entered a strong non-steady period (Stage 6).

The content on line 342-345 of the original manuscript has been revised as follows:

In the early period of Stage 3, aerosols were mainly submicron particles (0-1 μm). However, after the RH increased to 90% at 12:40 on March 25, a significant modal shift occurred in the aerosol particle size distribution. During Stage 3 (12:40-16:47 on March 25) and the early period of Stage 4 (16:47-19:30 on March 25), the proportion of particles with sizes of 0-1 μm decreased by 18% and 24%, respectively, while the proportion of particles with sizes of 1-2.5 μm increased by 5% and 4%, respectively, and the proportion of particles with sizes of 2.5-10 μm increased by 13% and 20%, respectively. This modal shift reflects the actual variation in the dry aerosol mass distribution. This is consistent with aerosols undergoing heterogeneous reactions (e.g., sulfate coating on dust surfaces) and aqueous-phase processing in the atmosphere. In the middle and late period of Stage 4, the proportions of particles with sizes of 0-1 μm and 1-2.5 μm showed increases, while the proportion of particles with sizes of 2.5-10 μm showed an overall decrease. This phenomenon was attributed to the gravitational settling and wet removal effect of large fog droplets. During Stage 5, the proportions of all particle sizes showed oscillating variation trends, and the PM mass concentrations showed an overall decrease. This indicates the dynamic competition between external transport and wet removal by fog droplets, ultimately resulting in the wet removal effect of fog on aerosols.

The content on line 430-435 of the original manuscript has been revised as follows:

In Fig. 6(b), during the dust passage (early period of Stage 2), the MEE decreased by 87% compared with the baseline before dust arrival. This indicates that the extinction efficiency per unit mass of dust aerosols was significantly lower under low RH conditions. As the RH increased (late period of Stage 2 to Stage 3), the MEE showed an increase. In the early period of sea fog formation (early period of Stage 4), the MEE increased by 2.3 times, reaching 125 m^2g^{-1}. During the sea

fog period (Stage 4), the MEE mostly remained between 70-120 m^2g^{-1}. This indicates the dominant contribution of fog droplets to extinction, keeping the visibility at low values. Subsequently, during the alternating evolution phase of advection sea fog and mist (Stage 5), the MEE showed an obvious decrease. This was related to the gravitational collision and wet removal processes of fog droplets. During the short-term sea fog disturbance in Stage 6, the MEE showed a peak value as high as 139 m^2g^{-1} again, increasing by 4.3 times. This further verifies that fog droplets have a strong extinction effect during the sea fog process. After entering the dissipation period, the RH continued to decrease. With the second invasion of dust, fog droplets disappeared and aerosols turned to dry state, and the MEE decreased rapidly.

- **L240: "… and the decreasing rate showed PM10 > PM2.5 > PM1." Does this mean that PM10 decreased the fastest? Is this estimated by eye or from a fit to the data?**

Answer: We thank the reviewer for this question. We clarify as follows:

(1) On whether PM_{10} decreased the fastest: this ordering means that, within Stage 5, PM_{10} had the largest relative decrease.

(2) On whether this was estimated by eye or from a fit: it is neither; the result is computed directly from the data. We take the measured PM concentrations at the beginning and end of Stage 5 and compute, for each size fraction, the relative decrease as (value at the beginning − value at the end) / value at the beginning, and then compare the three fractions, which yields the ordering $PM_{10} > PM_{2.5} > PM_1$.

(3) In addition, we noticed that the original wording "decreasing rate" was imprecise: since the quantity above is a relative decrease (a percentage) over the whole stage and is not divided by time, it is strictly not a "rate." We have therefore changed it to "relative decrease" and added the calculation method in the text, to accurately reflect the meaning of the quantity.

The content on line 240 of the original manuscript has been revised as follows:

The system attenuation began in Stage 5, which was still under the conditions of RH at 100% and stable southerly wind. The PM mass concentrations showed a decreasing trend, and the relative decrease (calculated as the difference between the values at the beginning and end of Stage 5 divided by the value at the beginning) followed $PM_{10} > PM_{2.5} > PM_1$. This was closely related to the efficient removal of coarse aerosol particles by the gravitational collision and wet deposition of fog droplets. The atmospheric visibility was basically maintained at about 1.0 km, consistent with the alternating evolution trend of advection sea fog and mist. In Stage 6, the stable southerly wind drove the RH to remain at 95%-100%. A dynamic balance was formed between warm and moist advection and highly hygroscopic aerosols. The mist state was maintained for 33 hours (visibility 2.0-4.0 km). A dense fog disturbance event of nearly 1 hour occurred during this stage. During 08:08-09:05 on March 27, PM_{10} suddenly increased to 131 $\mu g/m^3$. The visibility dropped sharply to 0.4 km. The wind speed increased to 5.8 m/s. After 09:25 on March 27, the northwest wind intruded. The intrusion of dry and cold air caused significant cooling. The RH dropped to the critical value of 95%. This caused the mist system to collapse (visibility increased to 4.0 km).

- **L252-245: Is this a simple comparison between the mean PM concentrations in stages 6 and 7? Is that appropriate given the PM spike in stage 6?**

Answer: We thank the reviewer for this expert comment. The reviewer is correct. L252–254 is indeed a direct comparison of the mean PM concentrations of each size fraction between Stage 6 and Stage 7. Stage 6 does contain a dense-fog disturbance spike lasting about one hour (08:08–09:05 on March 27, when PM_{10} briefly rose to 131 $\mu g/m^3$). To address the concern that this spike might raise the Stage 6 mean and thereby exaggerate the decrease, we carried out the following quantitative check.

Stage 6 lasts about 33 hours, whereas the disturbance spike lasts only about one hour, so its influence on the stage mean is limited. To verify this quantitatively, we recomputed the Stage 6 mean with the short spike period (08:08–09:05) excluded. The decreases of Stage 7 relative to Stage 6 are 32% for PM_1, 29% for $PM_{2.5}$, and 25% for PM_{10}, essentially the same as the results without excluding the spike (30%, 28%, and 25%). This shows that the comparison is robust and is not driven by the short-term spike in Stage 6.

The content on line 252-254 of the original manuscript has been revised as follows:

In the final Stage 7, driven by the continuously strengthening of the northwest wind, the dry and cold air mass completely replaced the warm and moist marine air mass. This caused the RH to drop from 95% to 77%, breaking the phase transition critical value of aerosols. In the early period from 17:50 to 19:00 on March 27, the wind speed increased from 6.4 to 9.0 m/s. This enhanced the turbulent vertical mixing and mechanically destroyed the residual fog droplets. The average mass concentrations of PM_1, $PM_{2.5}$, and PM_{10} in this stage decreased by 32%, 29%, and 25%, respectively, compared to those in Stage 6. The short-term dense-fog disturbance spike around 08:08–09:05 on March 27 was excluded when computing the Stage 6 mean so that the comparison reflects the overall background change. The visibility continued to increase to 30.0 km, indicating the irreversible dissipation of the mist system.

- **In Section 3.4, the interpretation does not match the results shown in Fig 10.**

- **L465-466: "With the establishment of [Stage 3]… TKE and u* first decreased and then increased." In the first half of Stage 3, TKE and u* are approximately constant. The "increases and decreases" are just noise.**

Answer: We sincerely thank the reviewer for this valuable suggestion. On re-examining Fig. 10, in the early period of Stage 3 TKE and u_* indeed remain approximately constant, and the variations within that period lie within the noise. Describing them as "first decreased and then increased" was an over-interpretation of noise and is not appropriate. The original sentence grouped U, TKE and u_* together as "first decreased and then increased," whereas in fact only U shows a clear, identifiable change (U increases to 4.67 $m \cdot s^{-1}$ by the end of Stage 3), while TKE and u_* show no such trend in the early period.

We have revised this description as follows. We have removed the "first decreased and then increased" statement for TKE and u_* and replaced it with a factual description. That is, in the early period of Stage 3, TKE and u_* remain approximately constant. In the later period, approaching the outbreak of sea fog, both increase. This enhancement of turbulence in the later period corresponds to the subsequent rapid formation of sea fog, which is the physical point intended in this passage. The revised description is consistent with the results shown in Fig. 10.

The content on line 465-466 of the original manuscript has been revised as follows:

Fig. 10 shows that TKE exhibited significant diurnal variation characteristics before dust passage (Stage 1), with a peak at 07:30 on March 24. This was mainly controlled by thermal buoyancy driven by shortwave radiation. However, with the passage of dust aerosols (Stage 2), the turbulence structure showed characteristics of dynamic enhancement and thermal stability. Although U, TKE, and u_* all showed an overall increasing trend, providing a strong mechanical shear source, ζ rapidly turned positive ($\zeta > 0$ for 60% of the time) due to the forcing of radiative cooling effect of the dust layer. This is consistent with the boundary layer inversion in physical mechanism. With the establishment of sea breeze (Stage 3), U increased to 4.67 $m \cdot s^{-1}$ at the end of Stage 3. In the early period of Stage 3, TKE and u_* remained approximately constant. In the later period, approaching the outbreak of sea fog, both increased. The stability parameter ζ was close to neutral. After the establishment of the sea breeze stability, the enhancement of turbulence promoted the rapid formation of sea fog.

- **L469-470: "During Stage 4… [the] turbulent intensity (Iv, Iw) was limited…" during this period, Iu and Iw are low but Iv is high.**

Answer: We sincerely appreciate the reviewer's rigorous and insightful question. I'm very sorry. Due to our carelessness, there was a mistake in the original manuscript here. On checking Fig. 10, during Stage 4 it is indeed I_u and I_w that are low, while I_v is high. The original text mistakenly wrote the limited components as (I_v, I_w), which should be (I_u, I_w). We have corrected this.

In terms of the physical mechanism, this correction is consistent with the explanation in this passage. Stage 4 is the sea-fog maintenance period, during which the boundary layer is strongly stably stratified (ζ positive), and the suppression is most pronounced for the vertical turbulence component (I_w), thereby restraining vertical mixing and entrainment and favouring the formation and maintenance of sea fog. Among the horizontal components, Iu is low while I_v is relatively high, indicating that the suppression of horizontal turbulence in this stage is directional rather than uniform. We have revised the text accordingly to specify the limited components and their physical meaning, so that the description is consistent with the results shown in Fig. 10.

The content on line 469-471 of the original manuscript has been revised as follows:

During Stage 4, the boundary layer showed strongly stable characteristics (ζ was all positive). The turbulence intensity (I_u, I_w) was limited, which was favourable for the formation and development of sea fog. In particular, the suppression of the vertical component (I_w) under the strongly stable stratification restrained vertical mixing and entrainment, which was related to the radiative cooling at the fog top and the long-term maintenance of boundary layer inversion (Fig. 8, 9). This result is consistent with the strengthening of stratification stability by negative Rn. Before 20:00 on March 25, TKE and U synchronously first decreased and then increased. At the same time, u_* remained at a high level, indicating that mechanical turbulence was relatively high. In the later period, TKE weakened accordingly with the decrease of U. Overall, this turbulence structure maintained the material exchange in the near-surface layer (supporting the hygroscopic growth of aerosols, the continuous interaction with fog droplets, and extinction with fog droplets). This also explains the observation results of the coexistence of continuously low visibility and multi-peak fluctuations of aerosol mass concentration PM during this period.

- **L491: "Finally (Stage 7) Iu and Iv remained at relatively high values." In this stage, Iv is lower than at any other time except perhaps Stage 1.**

Answer: We are very grateful to the reviewer for such a careful and expert check against Fig. 10. The reviewer's observation is entirely correct and very perceptive, and we sincerely apologize for this oversight. On re-examining Fig. 10, during Stage 7 I_v decreases markedly relative to the preceding stages and is indeed among the lowest values except for Stage 1. The components that remain high or increase in this stage are Iu and I_w. During Stage 7, I_u remains relatively high, I_w increases gradually, and Iv decreases markedly. We thank the reviewer once again for helping us identify this issue.

In terms of the physical mechanism, this correction is more consistent with the explanation in this passage. Stage 7 is the dissipation period, with the intrusion of dry-cold northwesterly winds. The longitudinal horizontal component I_u remains high owing to strong mechanical turbulence, the vertical component I_w increases (indicating enhanced vertical mixing and entrainment), while the transverse component I_v decreases. Together these reflect a reorganization of the turbulence components from the previous I_v-dominated structure, and the enhancement of the vertical component I_w corresponds directly to the dissipation of the sea fog. This is also consistent with the statement made earlier in the paper that the turbulence components underwent a rapid reorganization. We have revised the text accordingly, so that the description is consistent with the results shown in Fig. 10.

The content on line 491-493 of the original manuscript has been revised as follows:

In the morning of March 26 (Stage 5), although the stratification was still mainly stable, the resumed an upward trend of DSR (Rn turned positive) and the enhancement of local shear triggered intense instantaneous turbulence fluctuations (U instantaneously reached 5.43 m/s at 06:30, TKE reached 2.874 m^2/s^2, and u_* reached 0.756 $m \cdot s^{-1}$ at 07:00 on March 26). This fluctuation broke the previous quasi-steady equilibrium, accelerated the wet removal and collision of fog droplets, and promoted the transformation from dense fog to mist. Subsequently, the system entered a strong non-steady period (Stage 6). Especially during 06:30-09:00 on March 27, the sharp rise and turbulence parameters (U, u_*, TKE, ζ) corresponded to a dense fog disturbance. Then dry and cold northwest wind intruded. The turbulence intensity showed dramatic changes (I_v dropped sharply, I_u and I_w rose sharply). This indicates that the turbulence components underwent rapid reorganization. The vertical mixing efficiency improved, and the phase equilibrium was disrupted, while accelerating the evaporation and entrainment of fog droplets. After 09:00 on the 27th, U and TKE showed a sharp drop followed by a rapid increase trend before the end of Stage 6. This led the system to enter irreversible dissipation. The observation of the meteorological station showed that the ground was still in mist during this period. This indicates that the macroscopic dissipation of fog lagged behind the pulsation mutation of turbulence, showing a significant characteristic of turbulence acting first and fog responding later. Finally (Stage 7), I_u remained at relatively high values. At the same time, I_w gradually increased and I_v decreased markedly compared with the preceding stages. This indicated that the turbulence components underwent a reorganization, and that horizontal and vertical turbulent mixing and entrainment in the boundary layer became relatively active at this time, with strong turbulent exchange capacity. Dust again invaded, and the mechanical turbulent mixing dominated by dry and cold northwest wind further enhanced the momentum exchange in the lower atmosphere. At this time, the RH decreased significantly, the water vapor competition effect intensified, the phase equilibrium between aerosols and fog droplets was disrupted, causing the fog droplets to rapidly evaporate, and the system completely dissipated.

- **The interpretation of Fig 11 conflates observed ranges with thresholds**

- **This section identifies the ranges of turbulence parameters under which high PM10 concentrations and low visibility were observed, and describes these ranges as "thresholds." However, there is no evidence that if a dust intrusion occurred under different turbulent conditions, sea fog would not have formed.**

- **Only a narrow range of u* was observed, and this is interpreted as sea fog having an extremely high sensitivity to u*. This interpretation is unfounded. The dust intrusion happened to occur during a period of relatively constant u* but there is no evidence to suggest that this range of u* was required for fog formation.**

Answer: We greatly appreciate these two very valuable comments, which are of great help in improving the rigour of how our conclusions are stated. The two comments point to the same core issue, namely that we conflated an "observed range" with a "threshold" and, on that basis, made an unsupported inference about the sensitivity to u_*. We fully accept this, and respond in two parts below.

(1) On distinguishing an "observed range" from a "threshold." What this section (Fig. 11) identifies are in fact the ranges of turbulence parameters observed when visibility was low during the sea-fog maintenance period (Stages 4–6). The term "threshold" carries a causal connotation, namely that "if the turbulent conditions were outside this range, sea fog would not form," which our analysis is not sufficient to support. We have therefore changed all occurrences of "threshold" throughout the manuscript to "observed range," and no longer use expressions implying a causal criterion. This affects, among others, L497 and L503–508 of the main text.

(2) On the inferred sensitivity to u_*. The reviewer notes that the dust intrusion happened to occur during a period of relatively constant u_*, and that there is no evidence that this range of u_* was required for fog formation. We consider this to be correct. That u_* fell within the narrow range of 0.62–0.69 ms^{-1} is an observational fact, but inferring from it that sea fog has an "extremely high sensitivity to u_*" is indeed unfounded. We have therefore

deleted the expression "high sensitivity to u_*" from both the abstract and the main text, retaining only the objective observation that u_* fell within this range. This affects L23–24 of the abstract and L506 of the main text.

The content on line 22-24 of the original manuscript has been revised as follows:

Evolution mechanisms of explosive advection sea fog coupled with long-range dust transport over East Asia remain unclear. This study investigates a dust–advection sea fog event using ground-based observations, Himawari-9 satellite products, and ERA5 reanalysis data. Results show that dust may have undergone aging during transport, promoting sea fog under high humidity (RH>90%). Before sea fog formation (Stage 3: 12:40-16:47 on the 25th) and during the sea fog period (Stage 4: 16:47-19:30 on the 25th), the proportion of 0-1 μm particles decreased by 18% and 24%, respectively. The proportion of 1-2.5 μm particles increased by 5% and 4%, respectively. The proportion of 2.5-10 μm particles increased by 13% and 20%, respectively. This phenomenon is consistent with aerosols undergoing heterogeneous reactions and aqueous-phase processes, which may be associated with dust aging. Before fog formation, the cold air advection and radiative forcing of dust co-acted to deepen a 9°C inversion, which with warm-moist advection suppressed turbulent mixing and provided a favourable thermodynamic background for fog maintenance. The observed ranges of turbulence parameters (horizontal wind speed (U), turbulent kinetic energy (TKE), friction velocity (u_*), turbulence intensities (I_u, I_v, I_w)) were relatively distinct when sea fog maintains visibility within 1 km. The system showed a significant characteristic of turbulence acting first and fog responding later during the late stage of mist. The downward longwave radiation (DLR) was highly sensitive to changes in fog layer structure. Fog dissipation was caused by circulation adjustment and re-invasion of dry-cold dust carried by northerly winds, destroying phase equilibrium. These findings advance understanding of sea fog under complex aerosol backgrounds.

The content on line 497-498 of the original manuscript has been revised as follows:

To further clarify the observed ranges of turbulence parameters associated with sea fog, the relationships between PM_{10} mass concentration (representing total aerosol mass concentration) and key turbulence parameters (I_u, I_v, I_w, TKE, u_*, U) during Stage 4-6 were analysed (coloured by Vis) (Fig. 11).

The content on line 503-508 of the original manuscript has been revised as follows:

A clear result in Fig. 11 (a-f) all consistently show, when PM_{10} mass concentration exceeded 80 μgm^{-3}, Vis was mostly below 1 km. Based on this characteristic value, the observed ranges of turbulence parameters associated with maintaining sea fog below 1 km were also relatively obvious. The observed ranges of U and TKE were concentrated in 3.1-5.1 ms^{-1} and 1.91-2.74 m^2s^{-2}, respectively. It is notable that the u_* was limited to a significantly narrow range of 0.62-0.69 ms^{-1}. The observed ranges of I_u, I_v, and I_w were concentrated in 0.2-0.4, 0.8-0.95, and 0.21-0.31, respectively. This moderate turbulence threshold range established a quasi-steady dynamic equilibrium. This turbulence intensity was sufficient to maintain the co-suspension of high-concentration aerosols and fog droplets under near-saturated conditions. At the same time, it was effectively limited below the critical value, thus avoiding the dissipation of sea fog caused by stronger entrainment or mechanical turbulence at higher intensity.

- **Substantial weight is given to the aerosol composition inferred from the Himawari-9 aerosol product. However, this product is a model which assimilates observations, and given that (i) during the fog period, those observations are unavailable; (ii) the study area appears to be near the boundary between aerosol types at many timesteps (c.f. Fig 4); and (iii) the AOD is a column-integrated quantity and may not reflect near-surface composition, this speciation should be treated with skepticism.**

Answer: We are extremely grateful for the in-depth and professional comments from the reviewers. These three concerns are all very valuable and will help us more clearly define the applicable scope of the satellite

component data in this article. Based on the reviewers' suggestions and in combination with the revisions we have made, the responses are as follows in three points.

(1) On the unavailability of observations during the fog period. The original manuscript (data subsection, L143–146) already stated that, during sea-fog occurrences, the satellite retrievals may be filtered out or contaminated by cloud-screening mechanisms and the model outputs lack direct observational constraints, so the component-AOD product is used during the fog period only as a qualitative or semi-quantitative reference for the regional background. In response to the reviewer's comment, we have further clarified its quantitative limits of applicability by adding a statement in Section 3.2, namely that the satellite composition data are used as quantitative observations only during Stages 1–3 and Stage 7, and are limited to qualitative reference during the fog period (Stages 4–6); and we have removed the original statement that sulfate "contributed the most to sea fog" during the fog period, which gave the composition excessive weight, replacing it with a qualitative reference only. Importantly, the dust-aging inference in this study does not rely on the satellite composition data during the fog period (Stages 4–6).

(2) On the site appearing to lie near the boundary between aerosol types. We thank the reviewer for the close reading, and we would like to clarify a point that the original manuscript may have made misleading. Fig. 4 shows the aerosol distribution at only six specific time instants, and its purpose is to present the aerosol background of the event, the transport pathway of the dust, and the appearance of the secondary dust in the later period. To reflect the transitions between stages, the instants we selected are the times at which the successive stages are about to begin (e.g., the onsets of Stages 1, 2, 3 and 7), and these instants fall precisely within the transitional periods when the aerosol type is changing; consequently, in these particular panels the site appears to lie near the boundary between colour blocks. This is a feature of the selected time instants, not the general condition of the site throughout the event. In fact, the complete temporal evolution of the aerosol composition at the site is given in Fig. 5(a). As Fig. 5(a) shows, during the key period of dust transport (Stages 2–3) the dust AOD at the site rises markedly and dominates, so the site is mainly controlled by the dust signal rather than lying continuously on a type boundary. Fig. 4 is therefore used to characterize the large-scale spatial pattern and pathway of the dust transport, and Fig. 5(a) to represent the dominant temporal evolution of the composition at the site; together they support the assessment of the dust transport and background.

(3) On AOD being a column-integrated quantity that may not reflect near-surface composition. We fully agree. In response, we have added a statement in Section 3.2 clarifying that the satellite column AOD and the near-surface PM at 2 m represent information at different heights over the same site, and are complementary rather than contradictory. For example, during the pre-fog Stage 3, the satellite shows that the column dust AOD remained relatively high while the near-surface PM at 2 m had clearly declined; taken together, this indicates that the dust had not dissipated but remained suspended as fine particles above the 2-m sampling height, undergoing slow settling.

In addition, with regard to the reviewer's point that this product is a model that assimilates observations, we have added a clarification of its retrieval origin in Section 2.2, namely that only the total AOD is retrieved from H-9 while the partitioning into the five components is provided by the MASINGAR model and adjusted through total-AOD assimilation, so that readers can understand its nature and limitations.

Regarding the low credibility of AOD data during foggy periods, this has been explained in the original manuscript (Data Section, L143–146):

During sea fog occurrences, satellite retrievals may be filtered out or contaminated by cloud screening mechanisms. In this case, model outputs lack direct observational constraints. Therefore, during sea fog occurrences, this AOD data was mainly

used as a qualitative or semi-quantitative reference for the regional background aerosol environment. It was not used as an accurate observational basis for aerosol microphysical changes within the fog.

The content on line 142-143 of the original manuscript has been revised as follows:

For large-scale monitoring, L1 data from Himawari-9 (H-9), the new-generation geostationary meteorological satellite of the Japan Meteorological Agency (JMA), was used in this study. The satellite is equipped with the Advanced Himawari Imager (AHI), which has the capability of high-frequency and multi-spectral observations (Bessho et al., 2016). For fog area identification from the Himawari-9 satellite data, we adopted the brightness-temperature-difference (BTD) method, which is a widely used standard technique for nighttime fog and low-cloud detection (Kim et al., 2019). The BTD was computed as BTD=BT3.89-BT11.24, where BT3.89 and BT11.24 are the brightness temperatures at the mid-infrared (3.89 μm) and thermal infrared (11.24 μm) channels, respectively. Because fog and low-level water clouds differ in emissivity between the 3.89 μm and 11.24 μm channels, their BTD values differ from those of mid- and high-level clouds and of clear sky, allowing fog and low cloud to be distinguished from higher clouds. We note, however, that passive satellite detection cannot fully and unambiguously separate grounded sea fog from non-grounded low water clouds, since both are low-level liquid-water condensates with similar radiative signatures. Accordingly, the satellite identification is used in this study only to characterize the macroscopic spatial pattern and evolution of the fog area, while whether the observation site itself was within grounded sea fog is determined by the in-situ surface observations (visibility, RH and PM; see Section 3.1). For daytime periods, true-colour composites were utilized primarily for visual confirmation of the sea fog distribution, in which the fog area appears grey, spatially uniform and smooth-textured, with boundaries conforming to the coastline, relative to the surrounding clouds. For aerosol optical depth (AOD) data, the AHI L3 gridded aerosol product provided by JAXA Himawari Monitor (supported by the MASINGAR model system) was used. This product constrains the Meteorological Research Institute (MRI) aerosol transport model by assimilating AOD retrieved from H-9. Hourly AOD for components including sulfate, organic carbon, black carbon, sea salt, and dust can be output. Specifically, only the total AOD is retrieved from H-9. The partitioning into the individual aerosol components is provided by the MASINGAR model and adjusted through the total AOD assimilation. During sea fog occurrences, satellite retrievals may be filtered out or contaminated by cloud screening mechanisms. In this case, model outputs lack direct observational constraints. Therefore, during sea fog occurrences, this AOD data was mainly used as a qualitative or semi-quantitative reference for the regional background aerosol environment. It was not used as an accurate observational basis for aerosol microphysical changes within the fog.

The content on line 284-285 of the original manuscript has been revised as follows:

To further study the impact of aerosols on the formation and dissipation mechanism of this sea fog, based on the aerosol component AOD product of the H-9 satellite, the bilinear interpolation method was used to spatially interpolate the AOD onto the location of the observation site. The temporal variation characteristics of AOD for sulfate, black carbon, organic carbon, sea salt, and dust aerosols at Qingbang Island in the East China Sea were thereby calculated (Fig. 5(a)). Based on this, the average contribution rates of different types of aerosols during the entire study period were calculated (Fig. 5(b)). In this study, satellite derived aerosol composition data are utilized as quantitative observations during Stages 1–3 and 7, whereas they are limited to qualitative reference during the fog period (Stages 4–6).

The content on line 306-307 of the original manuscript has been revised as follows:

During the sea fog and maintenance stages (Stage 4-6), the sulfate AOD remained at a high level. This is consistent with the research results of Zhao (Zhao et al., 2022). However, these results are intended strictly as a qualitative reference rather than for quantitative identification. During the mist dissipation phase (Stage 7), the dust AOD increased significantly. This may cause cooling through the combined effect of scattering to reduce surface shortwave radiation and cold air. At the same time, it changed the stratification stability. This finally led to the evaporation of fog droplets, the increase of visibility, and the dissipation of mist. This further verifies the conjecture in Fig. 4 (e) and (f) that the dissipation of sea fog is related to the second passage of dust. In summary, dust aerosols may have played a dual role in this dust-sea fog event.

During the pre-formation phase of sea fog (Stage 3) and the mist dissipation phase (Stage 7), the temperatures both showed a decreasing trend. In Stage 3, when the RH increased, dust may have transformed into more hygroscopic mixed-state aerosols through the aging process, promoting the formation of sea fog. In Stage 7, when the RH decreased, dust inhibited the maintenance of mist.

The content on line 275-277 of the original manuscript has been revised as follows:

Form Fig. 4(a), the dust had not reached the observation site at 08:00 on March 24. At the same time, the aerosols at this site were mainly sulfate aerosols. In Fig. 4(b) at 15:00 on March 24, the dust originated from Mongolia and moved eastward through Inner Mongolia, Shaanxi, Shanxi, Jiangsu, and Shanghai to Qingbang Island in the East China Sea. This result is consistent with the sharp increase of aerosol PM mass concentrations at the near-surface observation site at 15:00 on March 24. This also confirms our conjecture that this increase was caused by dust passage. During Stage 2, the aerosols at this site were mainly dust particles. During Stage 2, the near-surface wind speed was relatively high and the turbulent kinetic energy was enhanced. This led to the strengthening of vertical mixing in the boundary layer. The dust in and above the boundary layer was fully mixed and settled to the near-surface. Therefore, the aerosol PM mass concentrations at the near-surface showed a significant sharp increase. From Fig. 4 (c) and (d), during Stage 3 (pre-formation phase of advection sea fog), dust always existed above the study area. The direct contribution to near-surface PM concentrations was relatively weakened. This indicates that dust aerosols were undergoing a slow settling process. It is necessary to clarify that in Stage 3, the PM mass concentration decreased relatively, referring to the reduction of the dust mass concentration at the near-ground 2 m level, rather than the dust being completely removed from the system. The dust did not disperse but remained suspended above the sampling height of the meteorological station and slowly settled. During Stage 3, the dust AOD remained at a relatively high level (Figures 4(c), (d)), while the PM at the near-ground 2 m level had significantly decreased (Figure 3). These two seemingly different observations are actually consistent. The meteorological station only samples at the 2 m height, which can only reflect the dry dust mass concentration near the ground, while AOD is the integral quantity of the entire column. Together, they indicate that the dust did not disperse but remained suspended in the air layer above the 2 m sampling height and was in a slow settling process. Therefore, the absence of detection at the 2 m level and the detectability of the entire column are manifestations of the complementarity of column observations and point observations, rather than contradictions. Fig. 4 (d) further shows that the dust at the observation site was weakening before sea fog formation. The high-value area of dust AOD was transported to northeastern China. Fig. 4 (e) and (f) indicate that during Stage 7 (dissipation phase of mist), dust passed through the observation site again, which may accelerate its dissipation.

The content on line 259 of the original manuscript has been revised as follows:

This analysis aimed to investigate whether the explosive increase of PM mass concentrations in Stage 2 was caused by dust transport passing through the observation site. It also explored whether dust had an impact on the evolution mechanism of sea fog. The AOD data of different aerosol types from H-9 were used. The distribution results of different aerosol types in different regions at typical moments during this event (Fig. 4). It should be noted that Fig. 4 shows the aerosol distribution at six specific instants, chosen at the onsets of the successive stages to illustrate the aerosol background, the dust transport pathway. Because these onset instants fall within periods when the aerosol type is in transition, the site appears in these particular panels to lie near the boundary between aerosol types. this reflects the selected instants rather than the general condition of the site throughout the event.

- **The causal links presented to explain the observations, and in particular the substantial role of dust in regulating fog formation, are unconvincing.**

- **The decrease in dust AOD and increase in sulfate AOD during Stage 3 is interpreted as dust becoming coated with sulfate. However, this could equally be explained by the advection of sulfate aerosol from anthropogenic sources after the dust passed by, especially given the fact that the PM peak had ended and that the current**

interpretation would require dust to arrive clean and then become gradually coated on-site, instead of mixing and ageing during transport from its source region.

Answer: We sincerely thank the reviewer for this valuable suggestion. This comment has helped us to describe more accurately how the dust aging occurs and where the sulfate comes from. We clarify and revise as follows.

(1) On how the dust aging occurs. We fully agree with the reviewer that the mixing and aging of dust do not begin on-site at the station, but occur during the long-range transport from the source region. For this event, we consider the aging of dust to be a continuous process, from the transport pathway to after the dust reaches the site. Part of the dust had already mixed with anthropogenic pollutants and undergone some degree of aging during long-range transport over polluted regions. This is consistent with the observation that the near-surface aerosol in Stage 2 was mainly concentrated in the 0-2.5 μm range. Another part of the dust had not yet been fully aged. After being transported over the observation site, it continued to age through heterogeneous reactions under near-saturated, high-humidity conditions. The view of this paper is therefore that the dust had already begun to age during transport before reaching the site, and continued to age after arrival, rather than arriving clean and then being coated on-site. The original wording may not have been clear enough and gave the impression of on-site coating, which was not our intention. We apologize for this and have clarified it in the text.

(2) On the decrease in dust AOD in Stage 3 and its relation to the PM. We would clarify that the decrease in dust PM in Stage 3 does not mean that the dust was removed or dispersed. The decrease of the near-surface PM at 2 m only means that little dust was detected at the 2-m level. AOD is a column-integrated quantity, and it reflects the information that the 2-m measurement cannot capture. The two are therefore complementary. In Stage 3, the column-integrated dust AOD remained relatively high (Fig. 4(c), (d); Fig. 5(a)). This indicates that the dust had not dissipated, but remained suspended above the 2-m sampling height and settled slowly. During Stage 2 to Stage 3, dust and sulfate co-existed in space and time, which provided the conditions for their mixing and chemical reactions.

(3) On the sources of the increase in sulfate AOD. We agree with the reviewer that part of the increase in sulfate AOD may come from anthropogenic sulfate transported by advection. More completely, we consider that the increase in sulfate AOD during Stage 3 may come from three contributions. The first is the sulfate already carried by the dust that had aged during long-range transport. The second is the sulfate that continued to form through heterogeneous reactions, such as Fe-S coupling, after the not-yet-fully-aged dust was transported over the site under near-saturated, high-humidity conditions (Zhuang et al., 1992; Duce et al., 1980; Martin et al., 1994; Li et al., 2025). The third is the sulfate advected from anthropogenic sources. These three contributions may co-exist. The advected anthropogenic sulfate is therefore not in conflict with the dust-aging process discussed in this paper, and does not rule it out. We also do not claim that all of the sulfate at the site comes from dust coating.

We must candidly acknowledge that this study did not have direct-observation single-particle chemical analysis and mixing-state characterization instruments (Scanning electron microscopy (SEM), Transmission electron microscopy (TEM) and Nanoscale secondary ion mass spectrometry (NanoSIMS)) that could directly demonstrate that the sulfate aerosol originated from aged dust particles coated with sulfate. For an island-type observation station such as Qingbang Island, deploying such large laboratory-grade single-particle aerosol instruments faces substantial practical challenges in terms of site space and equipment logistics. This is an objective methodological limitation of this study. Direct verification at the aerosol particle level necessitates concurrent single particle chemical and mixing state measurements during similar events in the future. This will be the primary direction of our future research.

The relevant content of the Fig. 5 analysis (lines 290–305 of the original manuscript) has been revised. The revised version is as follows:

From Fig. 5 (a) and (b), it can be seen that dust aerosol particles dominated and contributed the most during Stage 1-3(06:00 on March 25) before the outbreak of sea fog. The aerosol contributions from high to low were dust, sulfate, organic carbon, black carbon, and sea salt aerosols. It is notable that the contribution of sea salt aerosols was the lowest. This indicates that the aerosols at the observation site were mainly dominated by long-distance dust transport during this stage. During this stage, dust and sulfate coexisted spatially and temporally, which was conducive to their mixing and chemical reactions.

During the pre-formation phase of advection sea fog (Stage 3, 06:00-16:47 on the 25th), the dust AOD was gradually decreasing. The sulfate AOD was gradually increasing and became the dominant component. The contribution of sea salt remained at a low level. Previous studies have shown that in the marine atmospheric environment, Fe ions on the surface of dust can accelerate the formation of sulfate through the Fe-S coupling mechanism (Zhuang et al., 1992; Duce et al., 1980; Martin et al., 1994). This is highly consistent with the gradually increasing trend of sulfate AOD observed in our study. Previous studies have shown that dust particles can form a mixed structure of dust core and sulfate shell during the aging process. This internal mixing state can enhance the hygroscopicity of dust and effectively reduce the critical supersaturation required for its activation. This makes it easier to transform into cloud condensation nuclei (CCN) (Li et al., 2025; Tobo et al., 2010; Sullivan et al., 2009; Ma et al., 2013; Yin et al., 2007). In particular, Li et al. (Li et al., 2025) reported that, during the transport and aging of Asian dust, water-bearing secondary (sulfate/nitrate) coatings can form on the dust surface. Such coatings retain liquid water at ambient relative humidity and serve as a medium for aqueous-phase heterogeneous reactions, thereby markedly enhancing the hygroscopicity and activation ability of mineral dust. This mechanism is consistent with the dust-to-sulfate evolution observed before fog onset in the present event (Fig. 5). Such a scenario may have occurred during the event. It should be noted that the increase in sulfate AOD may come from three contributions. The first is the sulfate already carried by the dust that had aged during long-range transport. The second is the sulfate that continued to form through heterogeneous reactions, such as Fe-S coupling, after the not-yet-fully-aged dust was transported over the site under near-saturated conditions. The third is the sulfate advected from anthropogenic sources. In addition, the large accumulation of sulfate aerosols can cause a cooling effect on the atmosphere due to its negative forcing on solar radiation. Combined with the continuous moist advection, this further promotes the formation of sea fog.

A new paragraph (synthesizing the 5 observational points, literature deduction, and explicit uncertainty statement) has been added after Section 3.2 (in the original manuscript):

The results of Fig. 7 (a, b, c) all show that there was a typical exponential decay relationship between visibility and aerosol mass concentration. However, the decay rate was strictly controlled by the RH. During the low RH phase of dust passage (as shown in the blue-purple colour results at around 2-5 km in the figure), the sensitivity of visibility to PM concentration was relatively low. The exponential decay result showed a high exponential decay rate in the sea fog under high RH conditions. When the visibility was in the range of 0-1 km, the mass concentrations of PM_1, $PM_{2.5}$, and PM_{10} were in the ranges of 26-77, 38-157, and 47-275 μgm^{-3}, respectively. The low critical thresholds for sea fog occurrence were 26, 38, and 47 μgm^{-3}, respectively. This significant result indicates that only a low aerosol mass concentration is needed to trigger sea fog. This suggests that the aerosols are highly hygroscopic.

Combining the results of Figs. 4–7: (1) Fig. 4 shows that the dust was transported from Inner Mongolia through Shaanxi, Shanxi, and Shanghai to Qingbang Island in the East China Sea, passing through regions with elevated SO_2, NO_x, and NH_3 emissions. During long-range transport, dust readily reacts chemically with SO_2 and NO_x, which favours dust aging and sulfate formation. The chemical environment is consistent with the conditions required for heterogeneous sulfate formation on dust surfaces. (2) Quantitatively usable stages in Fig. 5: During the early periods of Stages 1–3 (before 06:00 on the 25th), dust and sulfate coexisted spatio-temporally, which was conducive to their mixing and chemical reactions. In the late period of Stage 3 (after 06:00 on the 25th, approximately 10.8 hours prior to fog formation), the sulfate AOD increased while the dust component AOD decreased. This scenario aligns well with existing literature reporting that dust aging and the Fe-S coupling mechanism accelerate sulfate formation (Zhuang et al., 1992; Duce et al., 1980; Martin et al., 1994). (3) Fig. 6(a) shows that during the dust passage period in Stage 2, the proportions of aerosol particles in the 0-1 μm and 1-2.5 μm size ranges increased significantly, with the aerosols mainly concentrated in the 0-2.5 μm range. As the dust transport

passed through regions with strong pollution emissions, the dust particles may have mixed and interacted with regional pollutants and undergone some degree of chemical aging. (4) Figs. 6(a, b) show that from late Stage 3 to early Stage 4, the modal shift reflected the evolution of dry aerosol particles rather than the direct effect of liquid water. This is consistent with the physical process in which aerosols, after undergoing heterogeneous reactions (e.g., sulfate coating onto dust surfaces) and aqueous-phase processing under near-saturated conditions in the atmosphere. Simultaneously, the MEE increased significantly by 2.3 times, reaching 125 m^2/g. This indicates that the extinction efficiency of aerosols in a wet state has significantly improved, which is consistent with the phenomenon that aerosols undergo hygroscopic growth in a high-humidity environment. These two independent observations jointly support that aerosols have undergone chemical and physical evolution in the atmosphere from different physical perspectives. (5) Fig. 7 shows that sea fog can be triggered at low PM_1, PM2.5, and PM_{10} mass concentrations, indicating that the aerosols possess relatively strong hygroscopicity. This is a reasonable speculation based on the combination of multiple observational results and the literature, rather than a microphysical mechanism directly verified in this study. Based on these five observational results, together with the literature on long-range transported dust particles (Li et al., 2025; Tobo et al., 2010; Sullivan et al., 2009; Ma et al., 2013; Yin et al., 2007) in which sulfate and nitrate coatings on the surfaces of dust particles have been directly observed as the literature reference. This study proposes the reasonable speculation that the transported dust may have undergone aging, with some particles becoming coated by sulfate to form internally mixed aerosols with a dust-core and sulfate-shell structure that exhibits strong hygroscopicity. This study did not have direct-observation single-particle chemical analysis and mixing-state characterization instruments (Scanning electron microscopy (SEM), Transmission electron microscopy (TEM) and Nanoscale secondary ion mass spectrometry (NanoSIMS)). These could directly demonstrate that the sulfate aerosol originated from aged dust particles coated with sulfate. For an island-type observation station such as Qingbang Island, deploying such large laboratory grade single particle aerosol instruments faces substantial practical challenges in terms of site space and equipment logistics. Direct verification at the aerosol particle level necessitates concurrent single particle chemical and mixing state measurements during similar events in the future. This will be the primary direction of our future research.

- **The observed changes in particle size distribution, MEE, and boundary layer stability are all explained with hypothesized causal mechanisms based on dust, without apparent consideration of alternate mechanisms. For example, the changing synoptic conditions presented in Fig 12 may be sufficient to explain Figs 9 and 10 without other mechanisms being required.**

Answer: We sincerely thank the reviewer for this constructive comment. The reviewer notes that our interpretation of several observations may rely too much on a dust mechanism without fully considering alternative mechanisms, and suggests that the synoptic-scale circulation itself may already be sufficient to explain the changes in boundary-layer stability and turbulence. We understand this concern, and we take this opportunity to state the basic position of the paper on the multiple contributing factors.

(1) On the multi-factor nature of sea fog. This paper treats sea fog from the outset as the product of multi-factor coupling, not something that can be brought about by any single factor. As stated in the Introduction, the life cycle of sea fog is controlled by more complex physical processes, and is the result of the nonlinear coupling of aerosol activation, condensation, radiation, turbulence, and thermodynamic and dynamic processes at multiple scales. The first paragraph of Section 3.5 also states that the regulating roles of local aerosols, radiation, and turbulence depend on the specific circulation background and air-sea conditions. We therefore consider that neither the synoptic system nor the dust alone is sufficient to explain the occurrence and evolution of sea fog, and the starting point of this paper is to use multi-source observations to describe how these factors co-evolve in the coupled process.

(2) On the relationship between the synoptic-scale circulation and the boundary-layer response. We agree that the synoptic-scale circulation provided the necessary large-scale background for this event. For Fig. 9, the formation of the inversion was indeed closely related to the synoptic-scale low-level cold advection (Fig. 12).

For Fig. 10, the stage-by-stage evolution of turbulence is in fact already described in the text in relation to synoptic processes, such as the land-sea breeze, the onset of warm-moist advection, and the intrusion of dry-cold northwesterly winds during dissipation, and we do not attribute it to dust alone. We would note that Fig. 12 describes the large-scale circulation background, whereas Fig. 9 and Fig. 10 describe the thermal and dynamic response of the boundary layer under this background. These are different levels within the same coupled chain, rather than competing explanations that replace each other. The synoptic-scale background alone does not directly give the strength of the near-surface inversion or the structure of the individual turbulence components, which still need to be revealed by high-frequency near-surface observations.

(3) On the role of the dust radiative effect. On the synoptic-scale background, the dust radiative effect is one link in this multi-factor coupling. Fig. 8 shows that, in the early period of Stage 2, DLR did not weaken with the decrease of solar elevation angle, but remained at about 335 $W \cdot m^{-2}$. This is consistent with the influence of the dust layer on the surface longwave budget through thermal radiation after shortwave absorption, and is difficult to explain by the synoptic-scale cold advection alone. We candidly acknowledge that, based on the near-surface single-site observations of this study, and without a radiative transfer model, we cannot quantitatively separate the contribution of the dust radiative effect from that of the synoptic-scale cold advection. This paper therefore does not claim that the inversion was caused by dust alone. We have already revised the near-surface cooling and the deepening of the inversion in Stage 2 in the text to be the joint result of the synoptic-scale cold advection, the solar diurnal cycle, and the dust radiative effect.

(4) On the particle size distribution and the MEE. For the modal shift in particle size in Fig. 6, it reflects the microphysical and chemical evolution of the aerosols themselves. This is at a different level from the synoptic-scale dynamic forcing, and the synoptic-scale circulation does not itself directly change the particle size distribution of the aerosols. For the MEE, its variation is mainly controlled by the relative humidity, which is largely regulated by the synoptic-scale warm-moist advection, and the role of the aerosols lies in their effect on the extinction efficiency at a given humidity. These two are therefore likewise not competing explanations with the synoptic-scale processes.

In summary, the position of this paper is not to explain all the observations by any single factor, but to follow the multi-factor coupling framework stated in the Introduction and Section 3.5, treating the synoptic-scale circulation, aerosols, radiation, and turbulence as irreplaceable links in the coupled chain. We thank the reviewer again for this comment.

The content on line 401-403 of the original manuscript has been revised as follows:

Fig. 8 shows that from Stage 1 to Stage 2, the radiation field evolved from the typical clear-sky diurnal characteristics to one accompanied by aerosol radiative effects. During Stage 2, the solar diurnal cycle together with the co-acting effects of cold-air advection and dust jointly modulated the attenuation of DSR at the surface. DLR did not weaken with the decrease of solar elevation angle, in the early period of dust passage, but remained at about 335 $W \cdot m^{-2}$. This observation is consistent with the influence of the dust layer on the surface longwave budget through thermal radiation after shortwave absorption. However, with sunset and the gravitational settling of dust, ULR showed an attenuation trend. Rn turned negative early at 17:30 on March 24, indicating that the surface energy budget reversed from surplus to deficit. In Stage 3, with the increase of sulfate aerosol concentration and its mixing with dust, aerosols showed strong scattering characteristics. Observations showed that DSR decreased by 744 $W \cdot m^{-2}$ from 12:30 to 17:00 on March 25. The decrease rate was 8% higher than that under clear-sky background (the same period in Stage 1-2). This further reflects that the radiative properties of different types of aerosols can change the surface-atmosphere radiation balance and heating or cooling rate, and then change the PBL structure. The strong scattering effect of sulfate aerosols combined with water vapor accumulation provided the necessary thermodynamic preconditions for the subsequent condensation and outbreak of sea fog in the near-surface layer.

The content on line 432-435 of the original manuscript has been revised as follows:

Fig. 9 shows that an inversion structure began to form in the near-surface layer at 10:00 on March 24, mainly concentrated at 0.4-1 km. Its occurrence and development were accompanied by both the synoptic-scale cold-air advection at low levels (Fig. 12(d-1)) and the continuous increase of dust AOD observed by satellite on March 24 (Fig. 5a). With the continuous passage and settling of the dust carried by the cold air, the near-surface inversion progressively strengthened. The maximum inversion reached 9 °C, and the thickness of the inversion layer also expanded significantly. This strong inversion layer was favourable for the accumulation of dust aerosols of sea surface and provided initial thermal conditions for the stabilization of the lower atmosphere. From 09:00 to 16:47 on March 25, with the establishment of sea breeze carrying warm and moist airflow over the cold sea surface, a continuously stable and deeper inversion layer formed in the boundary layer. This accelerated the continuous accumulation and physicochemical reactions of aerosols, providing sufficient CCN and ideal thermodynamic conditions for the outbreak of sea fog. During Stage 4 (advection sea fog period), warm and moist advection and the stable and deep inversion layer continued to exist. This is highly consistent with the continuous negative net radiation results at the near-surface. The combined effect of surface cooling and longwave radiative cooling at the fog top continuously strengthened the stability of the boundary layer, which was favourable for the formation and maintenance of sea fog. In Stage 5, there were signs of warming at the bottom of the inversion layer and the overall inversion intensity weakened, marking the beginning of the initial decay period of the system. At 06:00 on the 26th, the combined effect of the increase of DSR and turbulent mixing began to erode the cold air near-surface, causing some fog droplets to evaporate. This resulted in the oscillating characteristics of alternating between sea fog and mist. The thermal structure of the boundary layer became complex during the mist maintenance stage, with multi-layer thermal structures and instantaneous disturbances. This is consistent with the high-frequency fluctuations of radiation parameters SR, LR, and Rn. Finally, the original inversion structure had completely disintegrated, and a top-down mixing cooling process occurred. This may be related to large-scale synoptic systems. The intrusion of dry and cold air broke the warm, moist, and stable thermal conditions required for mist maintenance.

Technical Corrections:

- **L56: However, dust can undergo…**

Answer: We thank the reviewer for the careful reading. We have revised the wording at L56 of the original manuscript.

The content on line 56-62 of the original manuscript has been revised as follows:

Atmospheric aerosols play an important role in global climate by affecting the Earth-atmosphere radiation balance through direct or indirect effects (Huang et al., 2014; Bellouin et al., 2020; Liu et al., 2021). The interaction between aerosols and fog is rather complex and has similarities with the interaction between aerosols and clouds (Fan et al., 2016; Guo et al., 2018; Wang et al., 2023). As cloud condensation nuclei (CCN) (Twomey 1959), the concentration, size, and chemical composition of aerosols can significantly affect the microphysical and optical properties of fog (Jia et al., 2019; Yan et al., 2020; Dusek et al., 2006; Zhao and Garrett, 2015). Meanwhile, fog processes can also modify the evolution of aerosols (such as size, composition, mixing state, new particle formation, wet scavenging, etc.) (Schroder et al., 2015; Qian et al., 2023; Roth et al., 2016; Biswas et al., 2008). Numerous studies have shown that the increase in aerosol concentration can lead to higher fog droplet number concentration (Liu et al., 2021; Yan et al., 2020; Maalick et al., 2016; Stolaki et al., 2015) and fog top height (Liu et al., 2021; Stolaki et al., 2015), and may extend the fog lifetime (Quan et al., 2021; Yan et al., 2021). Currently, research on the interaction between sea fog and aerosols is still limited. Previous studies have mostly focused on sea salt aerosols acting as condensation nuclei for sea fog. However, spring is both the outbreak period of sea fog and dust. Studies have shown that dust from northern China and Mongolia can be transported over long distances across the Yellow Sea, East Sea, and even to the Pacific Ocean (Cahill et al., 2003; Sullivan et al., 2007). While traditional views

consider pure dust to be hydrophobic and inhibitory to fog formation (Li et al., 2025), dust particles can undergo significant atmospheric aging during transport. Through coagulation, cloud processing, and heterogeneous surface reactions, dust can mix with anthropogenic pollutants (e.g., ammonium sulfate, ammonium nitrate, biomass burning particles) (Li et al., 2025; Clarke et al., 2004; Korhonen et al., 2003; Yin et al., 2002; Zhang and Iwasaka, 2004; Zhang et al., 2003) as well as marine biogenic dimethyl sulfide (DMS) (Zhuang et al., 1992; Zhang et al., 2000). These complexes mixing substantially enhance the hygroscopicity of long-range transported dust (Li et al., 2025; Tobo et al., 2010; Sullivan et al., 2009; Ma et al., 2013; Yin et al., 2007). Due to the very complex interactions of multiple influencing factors between long-range transported dust and sea fog, the details of the effects of long-range transported dust on sea fog processes have not been well understood.

- **L65-82: This paragraph is rather scattered**

Answer: We thank the reviewer for pointing this out. We agree that the paragraph in L65-82 of the original manuscript was rather loosely organized. On review, this paragraph covers three aspects, namely the radiative effect, the role of turbulence, and the synoptic-scale modulation, but the transitions between these parts were missing and the order of a few sentences needed adjustment, which made it read as scattered. We have reorganized this part to make its logic clearer.

The content on line 65-82 of the original manuscript has been revised as follows:

The radiative forcing of aerosols can alter the thermodynamic and dynamic structure of the boundary layer (Deaconu et al., 2019; De Graaf et al., 2020), which can change the formation and dissipation conditions as well as the life cycle of fog. In fact, radiation is a key factor regulating the life cycle of sea fog (Fernando et al., 2021; Yun and Ha, 2022). The strong scattering and absorption of shortwave radiation by dust aerosols can cause significant cooling of near-surface atmosphere (Obiso et al., 2024; Wang et al., 2024). For advection sea fog, the classical theory mainly emphasizes the advection cooling mechanism, in which warm advection (warm-moist air flowing over cold sea surfaces) drives sensible heat loss, causing the air to cool and condense (Yang et al., 2024). However, under dusty conditions, can the radiative cooling induced by the aerosol layer promote the establishment of an inversion layer? There is still a lack of sufficient understanding. Inversion can provide stable stratification conditions for fog formation (Fitzjarrald and Lala, 1989; Holets and Swanson, 1981; Roach et al., 1976). However, research on the feedback mechanism between aerosol radiative effects and boundary layer thermal stratification has mostly focused on heavy pollution and haze processes over land. The role in marine advection fog remains unclear. Besides radiation, turbulence is another key dynamic factor regulating the sea fog life cycle. The observational and simulation studies have demonstrated that turbulence significantly influences the macrophysics of fog (Ye and Zhang, 2015; Porson et al., 2011), such as modulating the fog top height (Zhou and Ferrier, 2008). The effect of turbulence is twofold. Turbulence that is too weak is unfavourable for water vapor transport, while turbulence that is too strong leads to air entrainment and dissipation. Therefore, only moderate turbulence can promote fog development (Zhou and Ferrier, 2008; Price, 2019). Under the high aerosol background caused by the explosive input of dust, is there a moderate turbulence range for maintaining sea fog? Moreover, neither the radiative nor the turbulent processes act in isolation. The microphysical evolution and dynamic processes during sea fog do not exist in isolation. Their realization is inevitably controlled by the macroscale modulation of synoptic conditions and sea-air interface conditions (Yang et al., 2024; Dorman et al., 2021).

- **L75-77: The sentence beginning "In addition, …" has strange structure and should be revised**

Answer: We thank the reviewer for this careful comment. We have revised the wording at L75-77 of the original manuscript.

The content on line 75-77 of the original manuscript has been revised as follows:

Besides radiation, turbulence is another key dynamic factor regulating the sea fog life cycle. The observational and simulation studies have demonstrated that turbulence significantly influences the macrophysics of fog (Ye and Zhang, 2015; Porson et al., 2011), such as modulating the fog top height (Zhou and Ferrier, 2008).

- **L92: "laws" is not an appropriate word choice here**

Answer: We thank the reviewer for the comments. The wording at the locations mentioned by the reviewer was indeed problematic. At line 92, "laws" has been revised to "characteristics":

The aim of this study is to clarify the comprehensive driving mechanism of sea fog formation and dissipation in the dust aerosol environment by exploring the evolution characteristics of aerosol microphysics, radiation and boundary layer thermodynamic structure, turbulent dynamic characteristics, as well as synoptic conditions and air-sea conditions during this event.

- **L85: Instead of, "… turbulence, synoptic, and air-sea conditions" consider "…turbulence, and synoptic and air-sea conditions"**

Answer: We thank the reviewer for the comments. Based on your suggestion, we have made the revisions.

The content on line 85 of the original manuscript has been revised as follows:

How do aerosols, radiation, turbulence, and synoptic and air-sea conditions co-evolve in this complex coupling process?

- **L115: These links should be under "data availability" or in the reference section, not in the main manuscript text.**

Answer: We thank the reviewer for the comments. Based on your suggestion, we have made the revisions.

The content on line 85 of the original manuscript has been revised as follows:

The data used in this study include: (1) surface meteorological observation data; (2) radiation data; (3) near-surface turbulence observation data; (4) microwave radiometer retrieval data; (5) Himawari-9 satellite data; (6) ERA5 reanalysis data. The data sources and instrument descriptions are shown in Table 1.

- **Table 1: Abbreviations should be defined in a table caption.**

Answer: We thank the reviewer for this comment. We agree that a table should be self-contained, so that the reader can understand the abbreviations in it without referring to the main text. Although these abbreviations were already defined in Section 2.2, we fully agree that they should also be given with the table. Considering the limited space in the caption, we have added the definitions of all abbreviations used in Table 1 as a footnote below the table, so that the table can be read on its own.

The content on line 118 of the original manuscript has been revised as follows:

Data category	Instruments	Measurement parameters	Range/Accuracy	Interval
Weather Station data	AWS1900 Automatic Weather Station	T	-30-70 ℃ ± 0.1 ℃	10s
		RH	0-100% ± 2.5%	

		P_a	450-1100 hPa ± 0.1 hPa	
		WS	0.5-65 ms^{-1} ± 0.5 ms^{-1}	
		WD	0-360° ± 2°	
		PM	0-999 ugm^{-3} ± 10 ugm^{-3}	
		Vis	10-10000 m ± 5%	
Radiation data	CNR4-KIPZONE	DSR, USR, DLR, ULR	0-2000 Wm^{-2} ± 5%	1min
Turbulence data	CSAT3	u, v, w	± 0.04 ms^{-1} for horizontal ± 0.02 ms^{-1} for Vertical	10Hz
Microwave radiometer data	RPG-HATPRO	T	0-10 km	10s
Satellite data	Himawari-9	AOD	5 km	1h
		$BT_{3.89}$, $BT_{11.24}$	2 km	10min
Reanalysis data	ERA5(ECMWF)	MSLP, T_{2m}, u_{10m}, v_{10m} SST, Z_{850} d_{2m}	0.25°×0.25°	1h

*The air temperature (T) relative humidity (RH), pressure (Pa), wind speed (WS), wind direction (WD), particulate matter mass concentration (PM_1、$PM_{2.5}$、PM_{10}), visibility (Vis), downward shortwave radiation (DSR), upward shortwave radiation (USR), downward longwave radiation (DLR), upward longwave radiation (ULR), 3-D wind velocities (u, v, w), aerosol optical depth (AOD), mid-infrared brightness temperature ($BT_{3.89}$), thermal infrared brightness temperature ($BT_{11.24}$), mean sea level pressure (MSLP), 2-m air temperature (T_{2m}), 2-m dew point temperature (d_{2m}), sea surface temperature (SST), 10-m wind speed (u_{10m}, v_{10m}), and 850 hPa geopotential height (Z_{850}).

- **Eqn 1: Why specifically measure MEE using the mass concentration of PM2.5, as opposed to PM1 and/or PM10 which are also measured?**

Answer: We thank the reviewer for this very expert question. The reasons for using $PM_{2.5}$ as the denominator are as follows. First, both the direct extinction of the aerosol before fog and the aerosol that acts as condensation nuclei during fog are dominated by fine particles below 2.5 μm. For this event, the long-range-transported aerosol was mainly concentrated in the 0-2.5 μm range (Section 3.2). $PM_{2.5}$ therefore covers the particles that actually participate in extinction and activation. Using PM_{10} would include a disproportionate mass of 2.5-10 μm coarse particles, which have a low extinction contribution per unit mass and would artificially lower the MEE. Using PM_1 would omit the 1-2.5 μm particles. Second, $PM_{2.5}$ is the mass basis most commonly adopted for the MEE in aerosol optical and visibility studies, which facilitates comparison with previous work.

The content on line 155-160 of the original manuscript has been revised as follows:

The aerosol mass extinction efficiency (MEE) is a key parameter for characterizing the optical properties of aerosols. Its physical meaning is the scattering and absorption efficiency of light by particles with a unit mass concentration. It directly reflects the attenuation ability of aerosols on atmospheric visibility (Saide et al., 2022). Due to the lack of liquid water content data in this study, the MEE is defined as the ratio of the aerosol extinction coefficient (σ_{ext}) to the dry aerosol mass concentration:

$$MEE = \sigma_{ext} / \rho(PM_{2.5}) \quad (1)$$

$$\sigma_{ext} = 3912/Vis \quad (2)$$

Where σ_{ext} is the aerosol extinction coefficient with a unit of Mm^{-1}, $\rho(PM_{2.5})$ is the mass concentration of $PM_{2.5}$ with a unit of $\mu g \cdot m^{-3}$, and the unit of Vis is km. The factor 3912 in Eq. (2) equals 3.912×10^3, where 3.912 is the Koschmieder

constant (Lee and Shang, 2016) and the factor of 10^3 converts the extinction coefficient from km^{-1} (consistent with Vis expressed in km) to Mm^{-1}. The $PM_{2.5}$ mass concentration is used as the denominator because both the direct extinction before fog and the aerosols acting as condensation nuclei during fog are dominated by fine particles below 2.5 μm, which in this event were mainly concentrated in the 0-2.5 μm range (Section 3.2). The PM_{10} would add coarse-particle mass with low extinction per unit mass, and PM_1 would omit the 1-2.5 μm particles.

- **L161-172, Eqn 3-7: It would perhaps be more clear to start by describing the measured quantities, and then to describe the derived quantities afterwards.**

Answer: We thank the reviewer for this suggestion to improve the clarity of the presentation. We agree that it is clearer to first introduce the directly measured quantities and then the quantities derived from them. We have made the corresponding additions to the paragraph of Eqn 3 to Eqn 7 (L161-172). After introducing the sonic anemometer, we add a sentence stating that the high-frequency fluctuation data it measures are the three-dimensional wind velocities u, v, and w. After listing the turbulence intensity, friction velocity, turbulent kinetic energy, and stability parameter, we add a sentence stating that all these parameters are derived from the three-dimensional wind velocities u, v, and w. In this way the reader first understands the directly measured quantities and then the parameters derived from them.

The content on line 161-164 of the original manuscript has been revised as follows:

In order to study the evolution characteristics of turbulence during this event, high-frequency fluctuation data obtained from the 3-D Sonic Anemometer (CSAT3) was used. The measured high-frequency fluctuation data are the 3-D wind velocities (u, v, w). Turbulence-related parameters were calculated using the eddy covariance method (Zhou and Ferrier, 2008). These include turbulence intensity (I_u, I_v, I_w), horizontal mean wind speed (U), friction velocity (u_*), turbulent kinetic energy (TKE), and stability parameter (ζ). All these parameters are derived from the 3-D wind velocities (u, v, w). The calculation expressions of related physical quantities are as follows:

- **L174: Do not capitalize "fog"**

Answer: We thank the reviewer for this comment.

The content on line 174 of the original manuscript has been revised as follows:

3.1 Overview of dust-sea fog events

- **Fig 2: several comments.**

  - **Why are panels a and c a different type of image than b and d? This makes it look like the rows are pairs of (a,b) and (c,d) each showing the same scene with different instruments. If they same type of image is not available at all 4 timestamps, e.g. due to night vs day, clarify this in the caption.**

  - **The area shown in these maps is too large to see what is happening around the study site. It would be more useful to show a smaller region. (see also major comments)**

  - **Use different colours for coastlines and site identification, and don't make the site icon translucent – it is impossible to see without zooming in several times.**

  - **The site is identified by a star not a pentagram (need to correct caption)**

Answer: We thank the reviewer for the detailed comments on Fig. 2. We respond and revise point by point below.

(1) On panels a and c being a different type of image from b and d. The original caption was not clear enough. The situation is that the satellite channels and the identification method used for sea fog differ between day and night. During the day, solar reflected signals are available, so the visible channels are used to composite AHI RGB true-colour images for identifying sea fog, as in panels a and c. At night, there is no solar reflected signal and the visible channels are unavailable, so sea fog is identified by the brightness temperature difference between infrared channels, as in panels b and d. The four panels correspond to four different times, and are not paired to show the same scene. We have clarified this in the caption to avoid misunderstanding.

(2) On the map area being too large. We agree, and we have reduced the map domain of Fig. 2 so that the fog features around the observation site can be seen more clearly.

(3) On the colours of the coastline and the site marker, and the transparency of the site icon. We have revised these as suggested by the reviewer. The coastline and the site marker now use different colours so that they can be distinguished, and the site icon is no longer translucent but opaque, to ensure that it is clearly visible.

(4) On the name of the site symbol. The reviewer points out that the correct name is star rather than pentagram. We have corrected this in the caption.

The relevant content has been revised as follows:

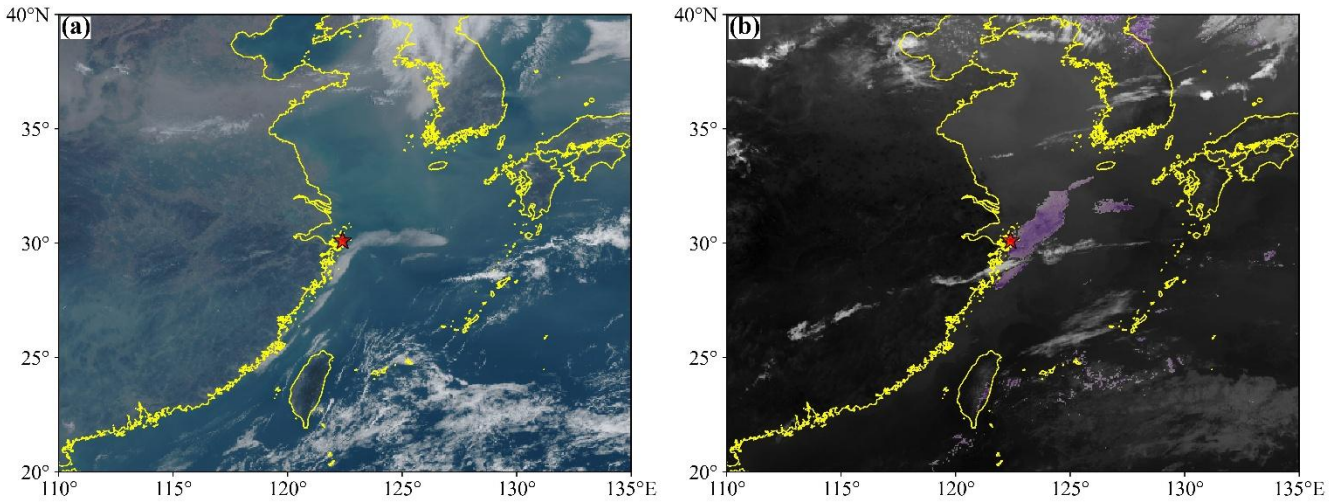

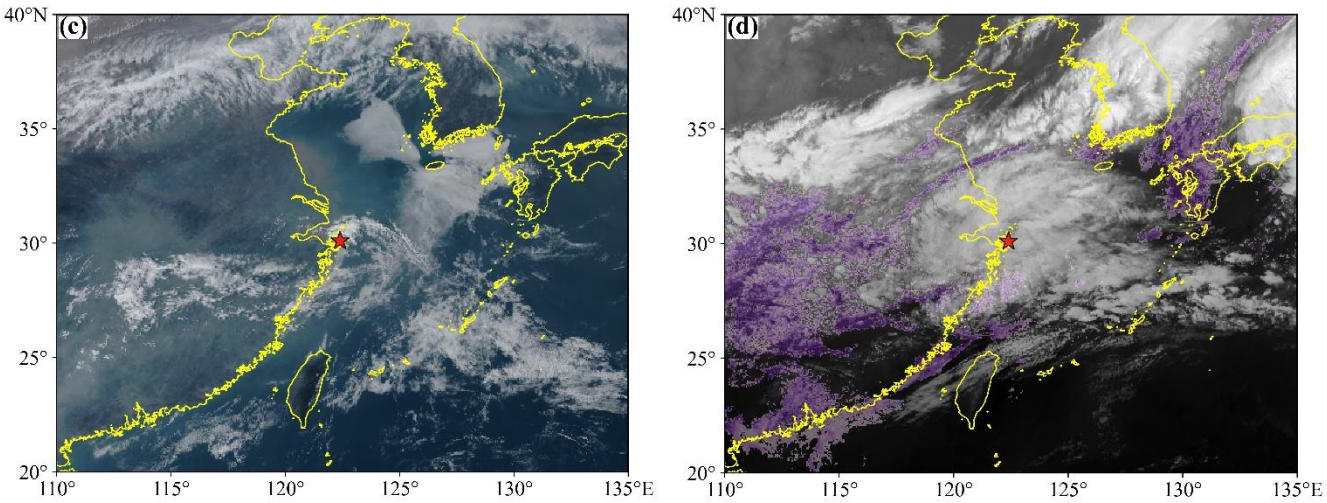

Figure 2: Sea fog monitoring images from the H-9 satellite at four different times. Sea fog is identified using different channels during the day and at night. a and c are the AHI RGB true-colour images composited from the visible channels at 09:00 LST on March 25 and 15:00 LST on March 26, respectively (local standard time (LST) = Universal Time Coordinated (UTC) + 8 h). b and d are the nighttime sea fog identification images obtained by the brightness temperature difference method using the infrared channels, since the visible channels are unavailable at night, at 18:00 LST on March 25 and 00:00 LST on March 28, respectively. Purple indicates fog identified at nighttime. The red star indicates the observation site.

- **Table 2: Would it be more valuable to list the visibility and RH minima and maxima instead of the values at the beginning and end of each stage? I am not sure what information the currently-listed ranges provide. Also, please specify whether "average" is a mean. Would a median be more appropriate?**

Answer: We sincerely thank the reviewer for these valuable comments on Table 2. We respond and revise point by point below.

(1) On the visibility and RH values listed at the beginning and end of each stage. we apologize that the meaning of these values was not clearly explained. We would clarify that these are not arbitrary ranges, but the visibility and RH values at the beginning time and end time of each stage. The seven stages in this paper are delineated according to the fog and mist criteria, namely the visibility and RH thresholds, and these beginning and end values are precisely what is used to delineate the start and end time of each stage of the event. Compared with the minima and maxima within a stage, the beginning and end values therefore serve more directly the purpose of stage delineation in this paper. We have clarified the meaning of these values in the main text.

(2) On whether the average is a mean and whether a median would be more appropriate. The values originally labelled as average in the table were arithmetic means. We fully agree with the reviewer that the median is more appropriate. This is because, within each stage, the visibility and RH may be skewed by short-term fluctuations, and the median is more robust to such fluctuations and better represents the typical condition of each stage.

The content on line 205- 206 of the original manuscript has been revised as follows:

Based on the fog identification criteria of WMO (WMO/GAW, 2003) and the UK Met Office (Met Office, 1994) (Vis < 1 km and RH $\geq 95\%$ is identified as fog, 1 km $\leq$ Vis $<$ 5 km and RH $\geq 95\%$ is identified as mist). This event was divided into 7 detailed stages (Table 2). Table 2 shows the sequence numbers, stage name, time, visibility, and relative humidity of the 7 stages. The visibility and RH values listed for each stage are the values at the beginning and end of that stage, which are used to precisely delineate the start and end time of each stage of the event. The measurement uncertainties of the near-

surface observations for stages 1–7 are based on the instrumental accuracies listed in Table 1. The magnitudes of the variations discussed below all exceed their respective measurement uncertainties. It should be noted that, although other cloud systems (including mid/high clouds and non-fog low clouds) coexisted near the observation site throughout the event in the satellite imagery (Fig. 2), the satellite imagery is used here only as a reference for the macroscopic spatial morphology of the fog. Whether the site itself was within grounded sea fog is determined by the surface observations: it is confirmed only when the in-situ visibility and RH satisfy the above WMO/Met Office criteria, in combination with the near-surface PM and other surface measurements (Fig. 3, Table 2). The coexistence of other clouds near the site in Fig. 2 therefore does not affect this surface-observation-based determination.

The content on line 207- 208 (Table 2) and relevant content of the original manuscript has been revised as follows:

Vis (km) (Median value), 4.8-2.5 (4.7), 2.5-3.7 (2.3), 3.7-1 (3.8), 0-1 (0.4), 1-2.3 (1.1), 2.3-4.5 (3.2), 4.5-30 (8.9).

Stage 2 was affected by strong external disturbance. The PM mass concentrations showed explosive increases during this period. The peak values of PM_1, $PM_{2.5}$, and PM_{10} at 17:08 on March 24 were 267, 460, and 469 μg/m³, respectively (an increase of 11-14 times). This trend is consistent with the explosive input characteristics of dust aerosols (Rodríguez et al., 2024). During this stage, the median visibility was 2.3 km and the relative humidity remained at a low level of 40-65% (Table 2).

- **L199, Fig 3: consider "variables" instead of "elements"**

Answer: We thank the reviewer for this comment.

The content on line 199 and Figure 3 of the original manuscript has been revised as follows:

The satellite monitoring results provided the overall spatial structure and evolution characteristics of this advection fog event. To clarify the specific evolution processes of various meteorological elements and atmospheric particulate matter during this event, a comprehensive analysis was conducted based on ground observation data of meteorology and pollutants. Fig. 3 shows the temporal evolution characteristics of mass concentrations (PM_1, $PM_{2.5}$, PM_{10}), atmospheric visibility (Vis), and main meteorological variables (relative humidity (RH), temperature (T), pressure (Pa), wind speed (WS), and wind direction (WD)) during the observation period.

Figure 3: Pollutant concentrations and meteorological variables during the observation period.

- **L205-206: "Based on…" is a sentence fragment. Further, it is unclear whether this paragraph is meant to define the 7 stages of the event; if so, it seems incomplete.**

Answer: We thank the reviewer for this comment. We have revised the text accordingly.

(1) On the sentence fragment. The sentence beginning with Based on was indeed a fragment and lacked a main clause. We have merged it with the following main clause into a single complete sentence, and rewritten the fog and mist criteria, previously given in parentheses, as a relative clause, so that the sentence is now grammatically complete and clearly expressed.

(2) On whether this paragraph is intended to define the seven stages. The purpose of this paragraph was not clearly stated. In the original text, only the criteria were given and the specific information on the stages was left entirely to Table 2, which made the paragraph appear incomplete. We have now added the names of the seven stages in this paragraph, namely the pre-dust phase (Stage 1), the dust phase (Stage 2), the pre-formation phase of advection sea fog (Stage 3), the advection sea fog phase (Stage 4), the alternating evolution phase of

advection sea fog and mist (Stage 5), the sustaining phase of mist (Stage 6), and the dissipation phase of mist (Stage 7), so that the paragraph is self-contained and the reader can understand the division of the stages without consulting the table.

The content on line 201-206 of the original manuscript has been revised as follows:

Based on the fog identification criteria of WMO (WMO/GAW, 2003) and the UK Met Office (Met Office, 1994), in which fog is identified when Vis < 1 km and RH ≥ 95%, and mist is identified when1 km ≤ Vis ＜ 5 km and RH ≥ 95%, this event was divided into 7 detailed stages (Table 2). Table 2 shows the sequence numbers, stage name, time, visibility, and relative humidity of the 7 stages. The seven stages are the pre-dust phase (Stage 1), the dust phase (Stage 2), the pre-formation phase of advection sea fog (Stage 3), the advection sea fog phase (Stage 4), the alternating evolution phase of advection sea fog and mist (Stage 5), the sustaining phase of mist (Stage 6), and the dissipation phase of mist (Stage 7). The visibility and RH values listed for each stage are the values at the beginning and end of that stage, which are used to precisely delineate the start and end time of each stage of the event. The measurement uncertainties of the near-surface observations for stages 1–7 are based on the instrumental accuracies listed in Table 1. The magnitudes of the variations discussed below all exceed their respective measurement uncertainties. It should be noted that, although other cloud systems (including mid/high clouds and non-fog low clouds) coexisted near the observation site throughout the event in the satellite imagery (Fig. 2), the satellite imagery is used here only as a reference for the macroscopic spatial morphology of the fog. Whether the site itself was within grounded sea fog is determined by the surface observations: it is confirmed only when the in-situ visibility and RH satisfy the above WMO/Met Office criteria, in combination with the near-surface PM and other surface measurements (Fig. 3, Table 2). The coexistence of other clouds near the site in Fig. 2 therefore does not affect this surface-observation-based determination.

- **L241: by "gravitational collision" do you refer to gravitational settling and dry deposition?**

Answer: We thank the reviewer for this question. What is referred to here is not gravitational settling or dry deposition, but the gravitational collection of aerosol particles by fog droplets, which is a wet scavenging process. The falling fog droplets, whose fall speeds exceed those of the aerosol particles, collide with and collect the particles as they fall, and coarse particles are collected more efficiently because of their larger inertia. We apologize that the original wording used gravitational collision and placed it in parallel with wet deposition, which was not sufficiently precise, since gravitational collection is itself a mechanism of wet scavenging. We have revised the sentence to refer to the wet scavenging by fog droplets, in which the falling droplets collect the particles through gravitational collection, so that the description is clearer.

The content on line 241-242 of the original manuscript has been revised as follows:

he system attenuation began in Stage 5, which was still under the conditions of RH at 100% and stable southerly wind. The PM mass concentrations showed a decreasing trend, and the relative decrease (calculated as the difference between the values at the beginning and end of Stage 5 divided by the value at the beginning) followed $PM_{10} > PM_{2.5} > PM_1$. This was closely related to the efficient removal of coarse aerosol particles by the wet scavenging of fog droplets, in which the falling droplets collect the particles. The atmospheric visibility was basically maintained at about 1.0 km, consistent with the alternating evolution trend of advection sea fog and mist. In Stage 6, the stable southerly wind drove the RH to remain at 95%-100%. A dynamic balance was formed between warm and moist advection and highly hygroscopic aerosols. The mist state was maintained for 33 hours (visibility 2.0-4.0 km). A dense fog disturbance event of nearly 1 hour occurred during this stage. During 08:08-09:05 on March 27, PM_{10} suddenly increased to 131 μg/m³. The visibility dropped sharply to 0.4 km. The wind speed increased to 5.8 m/s. After 09:25 on March 27, the northwest wind intruded. The intrusion of dry and cold air caused significant cooling. The RH dropped to the critical value of 95%. This caused the mist system to collapse (visibility increased to 4.0 km).

- **Fig 4: The figure would be easier to read if the caption was structured as, "Panels show the distribution of aerosol types at (a) 08:00 LST on March 24 (Stage 1: pre-dust phase), (b) 15:00 LST on March 24 (Stage 2: dust phase), …"**

Answer: We thank the reviewer for this suggestion, which improves the readability of the caption. We have adopted it in full. We have rewritten the caption of Fig. 4 following the structure suggested by the reviewer, listing the panel label, the corresponding time, and the corresponding stage one by one, so that the reader can directly match each panel with the time and stage it shows.

The revised content is as follows:

Figure 4: Panels show the distribution of aerosol types at (a) 08:00 LST on March 24 (Stage 1: pre-dust phase), (b) 15:00 LST on March 24 (Stage 2: dust phase), (c) 00:00 LST on March 25 (Stage 3: pre-formation phase of advection sea fog), (d) 15:00 LST on March 25 (Stage 3: pre-formation phase of advection sea fog), (e) 18:00 LST on March 27 (Stage 7: dissipation phase of mist), and (f) 18:00 LST on March 28 (Stage 7: dissipation phase of mist). In the figure, green, gray, red, blue, and yellow represent sulfate, black carbon, organic carbon, sea salt, and dust aerosols, respectively. The yellow star indicates the observation site.

- **Fig 5b: This should be a bar chart or stacked timeseries.**

Answer: We sincerely thank the reviewer for this excellent suggestion on data visualization. Following your valuable advice, we have replotted Figure 5(b) as a stacked-fraction plot (or stacked bar chart). This new visualization more accurately and intuitively illustrates the temporal evolution of the percentage contribution of each aerosol component, summing to 100% at any given time step.

The revised results of Figure 5(b) in the original manuscript are as follows:

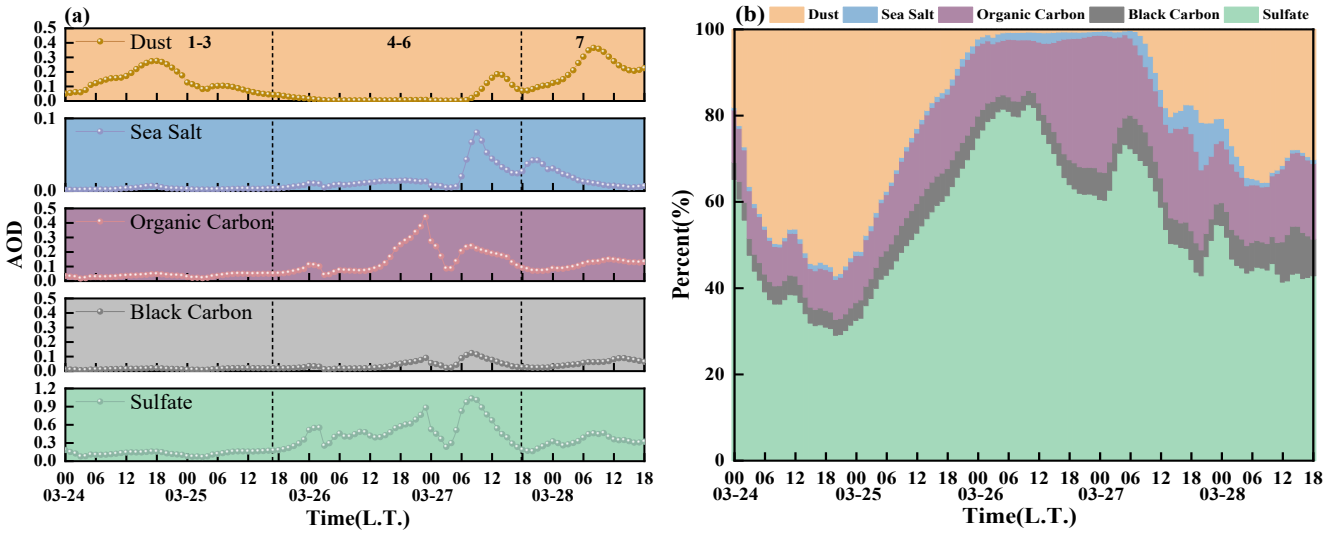

Figure 5: (a) and (b) show the temporal variation of AOD and the contribution rates of sulfate, black carbon, organic carbon, sea salt, and dust aerosols at Qingbang Island in the East China Sea, respectively.

- **Fig 9: Colorbar is missing a label. Also, the inversion layer appears to begin forming closer to 12:00 than 10:00 (L431).**

Answer: We thank the reviewer for the careful comments on Fig. 9.

(1) On the missing colorbar label. We have added a label to the colorbar, specifying the physical quantity and its unit, namely temperature and its unit.

(2) On the time at which the inversion layer begins to form. Having checked the temperature profiles retrieved by the microwave radiometer, the onset of the inversion layer is indeed at 10:00. We would note that the horizontal axis of Fig. 9 spans the whole event, a period of more than five days, so that the two hours between 10:00 and 12:00 occupy only a very narrow width in the figure and are difficult to resolve precisely by eye. This is likely the reason for the apparent discrepancy noted by the reviewer.

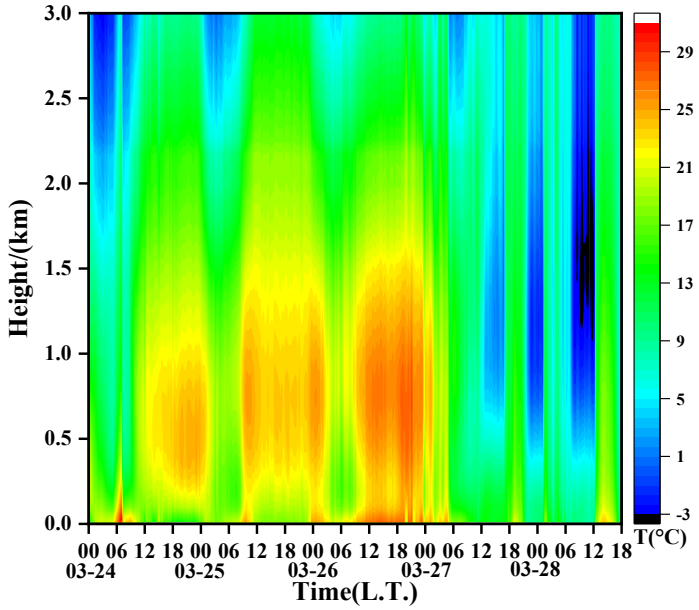

- **L504-505: Should this read, "sea fog with visibility below 1km"?**

Answer: We thank the reviewer for this suggestion. The original wording, maintaining sea fog below 1 km, omitted the physical quantity being referred to and was therefore ambiguous, as the reader might take it to mean a fog top height or fog layer depth below 1 km. Following the reviewer's suggestion, we have revised this to maintaining sea fog with visibility below 1 km, so that the expression is unambiguous.

The content on line 504-505 of the original manuscript has been revised as follows:

A clear result in Fig. 11 (a-f) all consistently show, when PM_{10} mass concentration exceeded 80 μgm^{-3}, Vis was mostly below 1 km. Based on this characteristic value, the observed ranges of turbulence parameters associated with maintaining sea fog with visibility below 1 km were also relatively obvious.

- **Fig 12: Please label colourbars. As in Fig 4, the caption would be improved by phrasing as "(a-k) the 850 hPa geopotential height (contour, gpm), (b-k) sea level pressure (contour, hPa), …"**

Answer: We thank the reviewer for these comments on Fig. 12.

(1) On labelling the colourbars. We have redrawn Fig. 12 with labels added to the colourbars, specifying the physical quantity represented by the shading and its unit, so that the reader can obtain this information directly from the colourbar when reading the figure.

(2) On the structure of the caption. We understand that the underlying purpose of the reviewer's suggestion is that the caption should clearly state the physical quantity, the plotting method, and the unit for each panel. This information is already given in full in the caption of Fig. 12, where the plotting method (contour, shading, or vectors) and the corresponding unit are specified in parentheses after each field.

We would also note that the panel labels in Fig. 12 follow a two-dimensional structure, in which the letters denote different physical fields and the number k denotes different times, so that each letter shows the same field at three different times. If the panels were listed linearly as suggested, the caption would read as follows.

(a-k) (k = 1, 2, 3) the 850 hPa geopotential height (contour, gpm) at three different times, (b-k) (k = 1, 2, 3) sea level pressure (contour, hPa) and RH (shaded, %) at three different times, (c-k) (k = 1, 2, 3) 2-m air temperature (shaded, °C) and horizontal wind (m/s) at three different times, (d-k) (k = 1, 2, 3) air-sea temperature difference (shaded, °C) and horizontal wind (m/s) at three different times.

As can be seen, the notations (k = 1, 2, 3) and at three different times would each have to be repeated after all four fields, four times in total, making the caption lengthy and repetitive. In the present caption, the four fields are listed together and the three times to which k = 1, 2, and 3 correspond, together with their stages, are then stated only once, which is both complete and concise. We have therefore kept the present labelling structure.

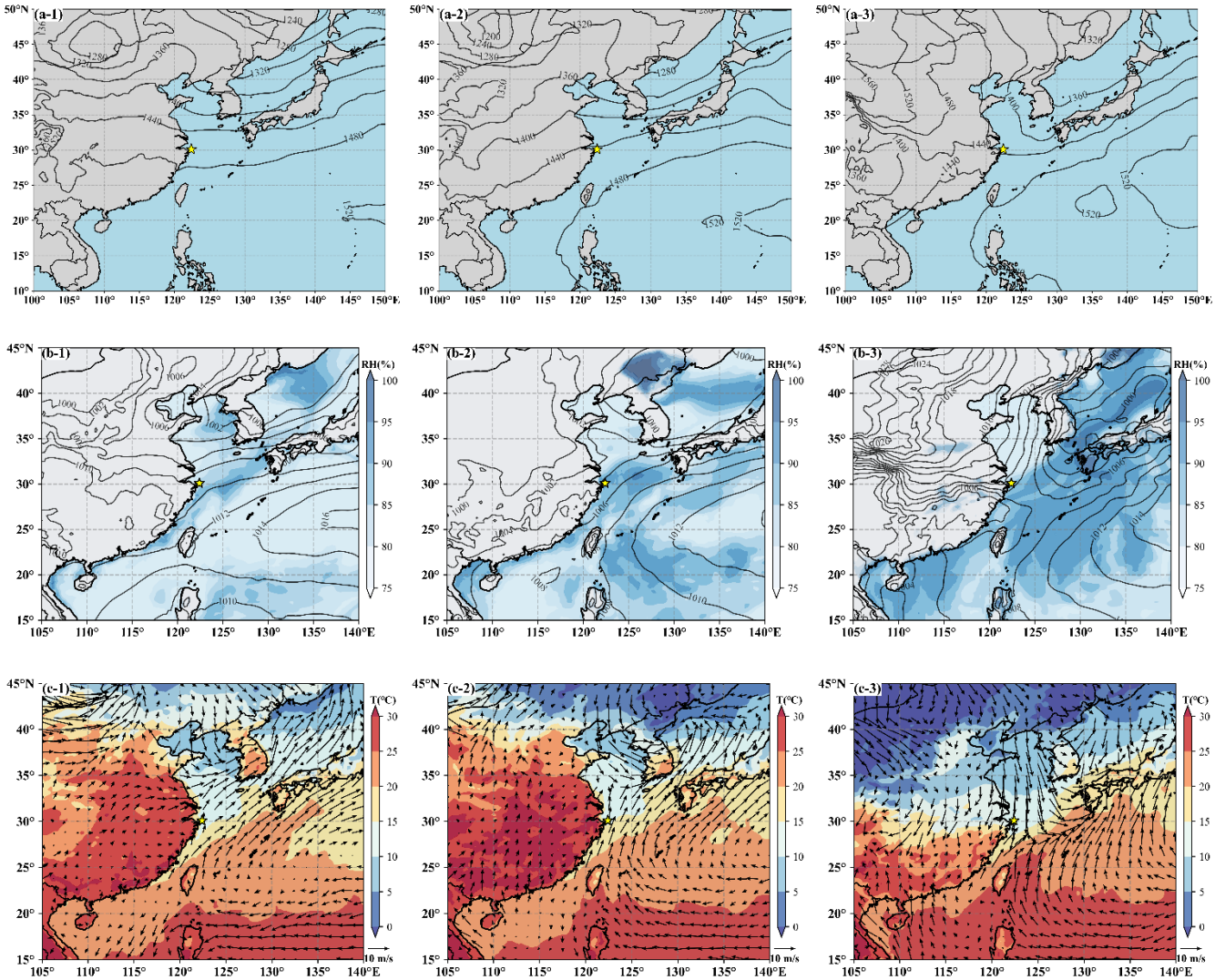

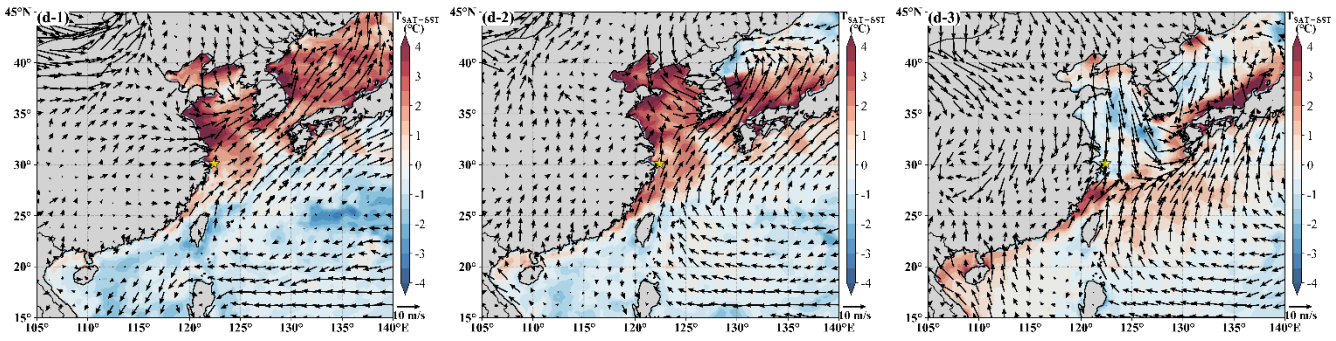

Figure 12: (a-k), (b-k), (c-k), and (d-k) (k=1, 2, 3) show the 850 hPa geopotential height (contour, gpm), sea level pressure (contour, hPa) and RH (shaded, %), 2-m air temperature (shaded, ℃) and horizontal wind (m/s), and air-sea temperature difference (shaded, ℃) and horizontal wind (m/s) at 3 different time, respectively. k=1 is Stage 2 (dust period) at 15:00 on March 24, k=2 is Stage 4 (advection sea fog period) at 17:00 on March 25, and k=3 is Stage 7 (mist dissipation period) at 18:00 on March 27.

- **L587: "… sulfate aerosols could replace sea salt as the dominant CCN…" Fig 5 indicates that there is more sulfate than sea salt at all times, so I am not certain that sea salt was ever the dominant CCN.**

Answer: We thank the reviewer for the careful comments. We apologize that the original wording was not rigorous. What we intended to convey was a contrast with the prevailing view in previous sea fog studies, in which sea salt aerosols are often regarded as the main CCN source for sea fog. In this event, the aerosols at the site were mainly controlled by long-range transported dust and its aging products, and the sea salt contribution was the lowest. We have removed the expressions replace and dominant CCN from L587 of the original manuscript, and now state that sulfate aerosols may act as one of the crucial CCN sources during this sea fog event.

The content on line 587 of the original manuscript has been revised as follows:

This event indicates that long-distance transported dust aerosols have a promoting effect on sea fog formation under high RH conditions. Dust aerosols originating from Mongolia passed through the observation site under the guidance of the westerly jet, causing the near-surface PM_{10} mass concentration to explosively increase to 469 μgm^{-3}. Different from the traditional view in sea fog research that sea salt aerosols act as CCN, this study found that during the Stage 3 to early Stage 4, dust and sulfate aerosols showed high coupling in time and space (sulfate AOD showed an increasing trend). During Stage 3 (12:40-16:47 on March 25) and early Stage 4 (16:47-19:30 on March 25), the aerosol particle size distribution showed obvious modal shift. The proportion of 0-1 μm particles decreased by 18% and 24%, respectively, while the proportion of 1-2.5 μm particles increased by 5% and 4%, respectively, and the proportion of 2.5-10 μm particles increased by 13% and 20%, respectively. This modal shift reflects the actual variation in the dry aerosol mass distribution. This is consistent with aerosols undergoing heterogeneous reactions (e.g., sulfate coating on dust surfaces) and aqueous-phase processing in the atmosphere. This also confirms that the cross-modal transformation of aerosols to fog droplets is the core microphysical cause of the sharp drop of Vis to below 1.0 km. The fact that aerosols with a low PM mass concentration threshold can trigger sea fog formation implies their strong hygroscopicity. Based on the independent observations above, and drawing analogies from existing literature on the aging of cross-sea dust, a reasonable speculation is that the long-range transported dust may have undergone aging over the ocean. Some dust particles might be coated by sulfate to form a "dust core–sulfate shell" aerosol structure, exhibiting strong hygroscopicity. Consequently, sulfate aerosols may act as one of the crucial CCN sources during this sea fog event. While this hypothesis has not yet been directly verified, it will serve as the primary focus of our future research.